Technische Universität München
Fakultät für Physik

Bachelorthesis

Dark Matter Annihilation in NGC 1068

Alexandra Scholz

30. September 2022

Erstgutachter (Themensteller): Prof. E. Resconi
Zweitgutachter: Prof. A. Ibarra

Contents

Abstract

There have been several astrophysical measurements and observations that prove the existence of Dark Matter (DM). If Dark Matter is of particle nature, the WIMP (Weakly Interacting Massive Particle), with an expected mass in the range of some GeV to TeV, probable by the IceCube telescope, would be a possible candidate. In this thesis, the neutrino flux from the spike and disk, generated from DM self-annihilation into Standard Model (SM) particles, of the barred spiral galaxy NGC 1068 was calculated. For this purpose, the Navarro-Frenk-White DM halo density profile was adopted. The calculation was performed for the DM masses 100 GeV, 1 TeV and 10 TeV and for an upper limit density slope γ=1.5 and lower limit slope γ=1. The neutrino energy spectra were simulated with the software Pythia, whereby the values for branch ratios and thermal averaged self-annihilation cross-sections are taken from the previously performed simulation of the relic density and indirect detection with MadDM. Comparing IceCube data from NGC 1068 with the results for those three masses, the TeV Dark Matter Annihilation scenario has no conflict on the spectrum shape from NGC 1068. Therefore, DM can be one of the potential explanation of the neutrino flux from NGC 1068.

Chapter 1

Introduction

Compelling evidences from observation and astrophysical measurements point to the fact, that our Universe consists of about 27% Dark Matter [1], which at this time cannot be explained by the current Standard Model. Several theories about the nature of Dark Matter are currently accepted in the physicist community. The most experimentally accessible assumption for a particle candidate for DM is the WIMP (Weakly Interacting Massive Particle), which has a mass in the range of several GeV/c^2 to TeV/c^2, probable by the IceCube neutrino telescope [2]. The WIMPs self-annihilation into Standard Model particles produces neutrinos, which could propagate undisturbed to earth and can be detected at telescopes. The neutrino flux from Dark Matter annihilation could give some enlightening hints about its nature. Even without detection, constraints on the DM model can be given from neutrino searches.
The telescope IceCube detects neutrinos coming from NGC 1068 and gets about one order of magnitude more neutrinos than gamma rays detected by FERMI [3] [4]. If the photons and neutrinos are produced by considering the standard scenario, the cosmic ray scenario, the same order of magnitude gamma rays and neutrinos are expected [5]. Absorption can affect gamma-rays but not neutrinos [6]. In order to interpret them for this observation, an alternative neutrino source or model should be considered.
In this thesis the neutrino flux from NGC 1068 is calculated by the method proposed in 1999, taking spike and disk into account, simulating the neutrino energy spectrum with Pythia and using the simulation software MadDM for dark matter observables set in in Pythia [7][8].
Having the results for the calculated neutrino flux from NGC 1068, it is then possible to figure out, if the measurement could be explained by Dark Matter annihilation. If the answer to this issue is yes, then a statement about the mass of the DM particle could be made.

Chapter 2

Theory

2.1 Nature of Dark Matter

2.1.1 Observational Evidence

The Standard Model, which has been one of the greatest successes of modern particle physics, does not describe all phenomena in the Universe. Only 5% of the total energy of the Universe correspond to the ordinary baryonic matter and are greatly explained by the SM. The other 95% are unknown, but suggested to consist of 27% dark matter and 68% dark energy by cosmological observations [1]. The name dark energy is given to the component of the material content, that changes slowly with space and time. The term Dark Matter was firstly used in 1932 by Fritz Zwicky, who inferred to invisible matter by studying the Coma galaxy cluster and, specifically, estimating how fast it rotates [9]. Nevertheless, there were astronomers in the early 19th century, like for example Friedrich Bessel [10], who had already considered dark stars or generally invisible matter in the form of dark nebulae or dark clouds [11].

Measurements of galaxy rotation curves have been possible since the 1960's and showed anomalies in observation and expectation. Including only the luminous mass, whose density decreases with distance from the center of the galaxy, one would obtain, using Kepler's laws, a theoretically calculated rotation curve that deviates very strikingly from the observed one. The circular velocity is expected to behave like

$$v(r) = \sqrt{\frac{GM(r)}{r}} \tag{2.1}$$

where the mass reaches its maximum outside the galaxy and remains constant. It would result, that with increasing radius the rotation speed decreases, as it is proportional to $\frac{1}{\sqrt{r}}$, however, one observes that the curve behaves differently. The comparison of the measured rotation curves of 21 different galaxies [12] showed that they all are flattened out with increasing radius. This fact would imply the mass scaling with r [13], which is consistent with the assumption of invisible particles acting like an ideal gas. The measured and in comparison the theoretical curve are

schematically represented in figure (2.1). If it is assumed that Kepler was right, then the discrepancy can be explained with non-luminous matter, which exists even in the outer regions of the galaxy [12][14].

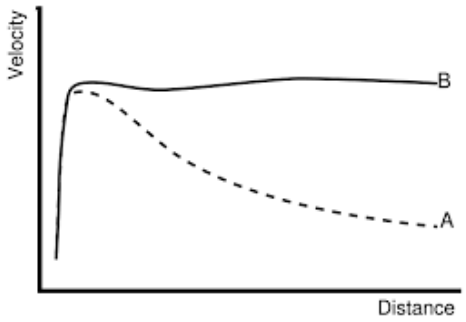

Figure 2.1: shematical illustration of calculated (A) and observed (B) rotation curve of a spiralgalaxy [15]

Another evidence can be found by looking at the gravitational lensing effect. It describes a deflection of the light of a distant object such as a galaxy, due to a massive object in front of it, for example a galaxy cluster. A distinction can be made in two types: strong and weak gravitational lensing. The object in the foreground is referred to as the lens. In the case of strong gravitational lensing, the mass of the lense is big enough, that the image of the object in the back is distorted to an arc, which are seen multiple times, also known as Einstein rings. For weak lensing, however, the mass is not sufficient for significant effects of a single background object, but the distortions of the objects in the background are still observable. It is necessary to take the distortions of many background objects into consideration. The mass distribution can be determined from the effect, giving a different result in observed mass and calculated, a direct hint to the existence of DM [16][17].

There are many other observations, which imply the existence of DM, but are not listed here. All these phenomena point to a mass-light ratio, that is much higher than it is obtained, if only the known and visible matter is included.

2.1.2 Candidates for Dark Matter Particles

It has been of great interest to explain and understand the phenomenon of Dark Matter, which has led to a variety of theories. In general there are three categories in which the they can be divided. The first one is based on Massive Compact Halo Objects (MACHOs) like planets, brown dwarfs and primordial black holes, that are responsible for DM [18]. Theories of modification of Newton's gravity law for

large scales (MOND), which do not need DM as an explanation, can be sorted in a second category [19]. Both categories do not assume a new type of particle, however, the third one does, which insists that the Standard Model is not complete and an extension is required.

The ΛCMD-Model, the Standard Model of Cosmology, is a model of the universe that consists of three components and is consistent with the theory of the Big Bang. The DM particle is required to be non-relativistic (cold) and also non-baryonic [2]. As a consequence it has no color and hence does not interact via strong force. In addition, the DM particle is electrically neutral. In general, the spin is not determined by observational evidences, so it can be fermionic or bosonic. It is assumed, that these particles were produced thermally in the early universe and the relic abundance today was set, when they got out of equilibrium with the high temperature plasma. With the expansion of the universe, the density of the particles and antiparticles decreased. The self-annihilation rate became smaller than the thermal-averaged expansion rate. One speaks of the freeze out of the relative density of Dark Matter. With the knowledge of the relic abundance of DM via thermal production today, this results in a thermally averaged self-annihilation cross-section of $\langle \sigma v \rangle = 3 \cdot 10^{-26} \frac{\mathrm{cm}^3}{\mathrm{s}}$ [8].
There exist three categories, in which the extensions of the standard model can be divided. The first one is the theory of Axion like particles (ALPs) [20] and the second extension is based on results of the theories of the Universal Extra Dimensions (UED) [21]. The third type is the supersymmetric extension (SUSY) of the SM, which requires a symmetry between forces and matter and predicts a superpartner for each particle in the SM. SUSY is an interesting point of research even outside of the DM problem. It converts a boson into a fermion and vice versa. In detail there is a fermion with spin $1/2$ for each boson and a scalar boson for each handedness fermion [22][23]. For the CDM (Cold Dark Matter) scenario the weakly interacting massive particles (WIMPs) are considered as candidates for DM [8].
In this thesis, WIMPs, with the mass between 100 $\mathrm{GeV/c^2}$ and 10 $\mathrm{TeV/c^2}$ are considered as Dark Matter particle candidates.

2.2 Dark Matter Annihilation

The self-annihilation of Dark Matter particles in particles of the Standard Model is possible, implied by the thermal production of weakly-interacting dark matter [8].

The produced particles are expected to decay into lighter ones. Neutrinos are generated when muons and tauons decay into lighter particles. Bosons are supposed to decay either into leptons or quarks, which then will hadronize into mesons. The

mesons then decay leptonically or into photons. In general, at the annihilation of DM into heavy states like quarks, muons or weak bosons, a neutrino signal is generated. These neutrinos can then propagate undisturbed to the earth and can be detected, for example by neutrino telescopes such as IceCube (Chapter 2.2.2.4.). There is also the direct annihilation into neutrinos, where its energy corresponds to the rest mass of the DM particle, i.e. $E_\nu = m_\chi$ [8].

$$\chi\chi \to \nu\bar{\nu} \tag{2.2}$$

Neutrinos are electrically neutral leptons, which have no mass in the Standard Model and are only subject to the weak interaction. From observed decays, as for example the decay of charged pions, one recognizes that the resulting muonneutrino or antimuonneutrino behaves in such a way that only reactions are induced, in which muons or antimuons are produced and no electrons or tau leptons. Therefore it becomes clear that there are three different flavours, thus the six leptons can be divided into three lepton families corresponding to it.

$$\begin{pmatrix}\nu_e\\ e^-\end{pmatrix}, \begin{pmatrix}\nu_\mu\\ \mu^-\end{pmatrix}, \begin{pmatrix}\nu_\tau\\ \tau^-\end{pmatrix} \tag{2.3}$$

Experiments like the β-decay are also consistent with neutrino and antineutrino being two different particles. However, there is a theory that neutrinos could be Majorana particles, which would mean that particle and antiparticle are equal.

$$\left(\nu_{e\uparrow}, \nu_{e\downarrow}\right) \tag{2.4}$$

Here the arrow stands for positive or negative helicity. This could be proved by the observation of the neutrinoless $\beta\beta$-decay, which would also prove that the neutrinos have masses different from zero. Nevertheless, it is already clear from oscillation experiments, such as Superkamiokande [24] and SNO [25], that they have a non-zero mass and can transform into each other, i.e. change their flavor [26]. Still, as neutrinos are the most weakly interacting particles, they are also the hardest to detect. As a consequence, models for DM annihiliation directly into neutrinos, are difficult to rule out [8].

2.2.1 Dark Matter Halo Density Profiles

A very important role in the calculation of the neutrino flux is played by the structure of the CDM halo. The connection between the rotation curve of a spiral galaxy and the structure of the halo is tight. The Dark Matter halo profiles can be probed for inner masses by rotation curve measurements.

To construct a model, which describes the structure, it is necessary to choose a descriptive function. It makes sense to take the density profile, because of a decisive reason: the most important functions, which define a galactic system, like the gravitational potential, cumulative mass profile and the surface mass density, are integrals over the density profile. There are some conditions, necessary to be satisfied, for the physical model. First, the density must always be positive and finite. In addition, it must be a function that decreases uniformly with increasing radii and approaches zero for large ones. Furthermore, there must be several finite moments, especially those that determine the central gravitational potential, the total mass, and the effective system radius. The last point to mention is, that the function must not exhibit jump discontinuities [27]. The different, most common, Dark Matter halo density profiles are shown in figure 2.2.

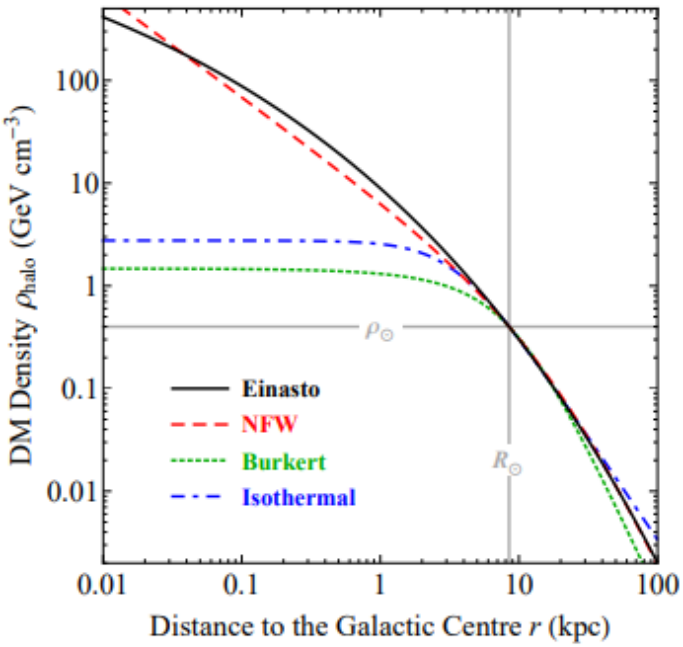

Figure 2.2: Comparison of different DM halo density profiles [28].

The non-singular Isothermal profile is a tempting distribution assumption and is defined by the finite central density ρ_0 and a the core radius R_c. It is based on the

theory, that the gravitational collapse leads to the formation of virialized spherical halos with isothermal profiles [29].

$$\rho_{Isothermal}(R) = \frac{\rho_0}{1 + \left(\frac{R}{R_c}\right)^2} \tag{2.5}$$

As it can be seen in the graphic and in the formula 2.5, it is assumed that the density remains more or less flat up to the core radius, i.e. that there is a core with constant density. The circular velocity is given by:

$$V^2_{circ,iso}(R) = \frac{GM(R)}{R} = 4\pi G\rho_0 R_c^2[1 - \frac{R}{R_c}\arctan\frac{R}{R_c}] \tag{2.6}$$

where M is the mass within the radius R [30].

The assumption of an inner core is also made in the Burkert profile. This theory is based on fundamentals, observed rotation curves of dwarf galaxies, in which dark matter dominates. It is a empirical law similar to a pseudo-isothermal distribution, also defined with the two paramters ρ_0 and R_c [31].

$$\rho_{Burkert}(R) = \frac{\rho_0 R_c^3}{(R + R_c)\cdot(R^2 + R_c^2)} \tag{2.7}$$

The profile is not valid for big distances to the center, but represents a good fit until the viral radius, within which the virial theory (2T+U=0, with T the the total kinetic energy of a self-gravitating body due to the motions of its constituent parts and U the gravitational potential of the body [32]) is valid [33].

The Einasto and the Navarro-Frenk-White (NFW) profiles are fundamentally different to the Isothermal and Burkert one as can be seen in figure 2.2. Unlike the last described models, the next two do not have a core, but work with the assumption of a cuspy Dark Matter distribution. Starting with the Einasto, which is defined by a power-law logarithmic slope [34]

$$\gamma = -\frac{dln\rho(R)}{dlnR}(R) \propto R^{\frac{1}{n}} \tag{2.8}$$

and with integrating 2.8 is given by:

$$\rho_{Einasto}(R) = \rho_s \exp[-d_n[\left(\frac{R}{R_{sph}}\right)^{\frac{1}{n}} - 1]] \tag{2.9}$$

R_{sph} is the sphere radius, which contains half of the total mass. The constant d_n makes sure that it really is half within R_{sph}. It was applied on galaxies with models,

which were multi-component, for each component there is a certain set of parameters (R_{sph}, ρ_s, n). In the equation, n is the Einasto index and specifies the steepness of the power-law. For dwarf galaxies to clusters the value lies between around 4.54 and 8.33 [35] and decreases with mass and redshift in the Millennium Run [36]. A multi-component Einasto profile was used for fitting the surface brightness profiles of elliptical galaxies in the Virgo cluster with two or three components and the result was, that the values of n for the outer component (5<n<8) are consistent with N-body simulations for Dark Matter halos. Additionally, for the Einasto component with n between 5 and 8, the statement is made that those are Dark Matter dominant [37]. Due to the good agreement with observations, there is also great interest in detailed properties of the Einasto profile [38].

The already mentioned NFW profile is the only CDM halo profile, which comes from N-body simulations. Navarro, Frenk, and White claimed that DM halos cannot be well approximated by isothermal spheres, but have a slightly varying logarithmic slope [39]. From the results of N-body simulations, they obtained a universal profile for masses between dwarf galaxies and galaxy clusters. The numerical experiments are based on the simulation of 19 different systems, with masses over four orders of magnitude and selected circular velocities ($100\frac{\mathrm{km}}{\mathrm{s}}, 250\frac{\mathrm{km}}{\mathrm{s}}, > 450\frac{\mathrm{km}}{\mathrm{s}}$). The non-abitrary choice comes from the indication of the cosmic scattering. The evolution of 262,144 particles in periodic boxes, which stops when the rms fluctuations in spheres with radius 16 Mpc was $\sigma_8 = \frac{1}{b} = 0.63$, which is supposed to represent the present, are taken into account. It turns out that collapsed systems with different masses, whose centers are defined as centers of halos, can be found. An average overdensity of 200 was measured in each case. The radius enclosing the sphere with an average density 200 times greater than the critical density of the universe is called the virial radius R_{200}. In other words, this is the radius within which the virial theory is valid, i.e. that the kinetic energy is equal to half of the potential energy. Then the particles in the 19 systems are traced back to the original time. The size of the box, the high resolution box containing all of them, was chosen in order to obtain all systems at redshift z=0 with the same size. A N-body code was used for all simulations. This is a second order accurate, nearest-neighbour, binary-tree code with individual particle timesteps. The effects of numerical limitations were tested on the lightest ($M = M_{\odot}10^{11}$) and most massive ($M = M_{\odot}10^{15}$) halos. The choice of the decisive parameters like the number of particles, initial redshift, gravitational softening and the timesteps have no influence [39]. As a result a universal CDM halo density profile was obtained: [39] [40]

$$\frac{\rho_{NFW}(R)}{\rho_{crit}} = \frac{\delta_c}{\frac{R}{R_s}(1+\frac{R}{R_s})^2} \tag{2.10}$$

Here R_s is the characteristic scale radius, where the mass density profile changes density slope between inner and outer parts of the galaxy. It can be expressed via the dimensionless concentration c and the virial radius R_{200}:

$$R_s = \frac{R_{200}}{c} \tag{2.11}$$

The critical density of the Einstein-de-Sitter Universe can be calculated with the current Hubble constant H and the gravitational constant G:

$$\rho_{crit} = \frac{3H^2}{8\pi G} \tag{2.12}$$

and the characteristic overdensity is given by:

$$\delta_c = \frac{200}{3} \frac{c^3}{(ln(1+c) - \frac{c}{1+c})} \tag{2.13}$$

A more generalized way to express the profile is over the density slope γ and the characteristic density ρ_s [8]:

$$\rho_{NFW}(R) = \rho_s \frac{2^{3-\gamma}}{(\frac{R}{R_s})^\gamma (1 + \frac{R}{R_s})^{3-\gamma}} \tag{2.14}$$

The mass within the virial radius is simply [41]:

$$M_{200} = 200 \cdot \rho_{crit} \frac{4\pi}{3} R_{200}^3 \tag{2.15}$$

Further the mass can also be determined by the integrating over ρ_{NFW}.

$$M_{200} = \int_0^{R_{200}} 4\pi R^2 \rho_{NFW}(R) dR = \int_0^{R_{200}} 4\pi R^2 \rho_s \frac{2^{3-\gamma}}{(\frac{R}{R_s})^\gamma (1 + \frac{R}{R_s})^{3-\gamma}} \tag{2.16}$$

The identical information about the structure is given with the circular velocity profile. The simulated circular velocity curves are all very similar. At the center they rise, remain almost constant for a certain region and finally decrease near R_{200}. More massive halos show a curve, which rises to a larger fraction of the virial radius than smaller halos. Important facts, which can be seen, are that the maximal circular velocity V_{max} is significantly larger than the one at the virial radius V_{200} and for low mass systems the ratio $\frac{V_{max}}{V_{200}}$ is even larger. A larger fraction of the virial radius is given for the radius, at which the velocity is maximal for larger systems. The conclusion is, that low mass systems are more concentrated, because they formed

earlier, when the density of the universe was higher. The circular velocity in the NFW profile can be calculated with [39]:

$$\left(\frac{V_c(R)}{V_{200}}\right)^2 = \frac{1}{x}\frac{ln(1+cx) - \frac{cx}{1+cx}}{ln(1+c) - \frac{c}{1+c}} \tag{2.17}$$

with $x = \frac{R}{R_{200}}$. It reaches its maximum at $R_{max} = 2R_s = \frac{2R_{200}}{c}$. The two parameter V_{200} and c characterize the CDM halo over the NFW profile and are even correlated with each other. The maximum of the circular velocity can be written in:

$$\frac{V_{max}}{V_{200}} = \left(\frac{0.216c}{ln(1+c) - \frac{c}{1+c}}\right)^{\frac{1}{2}} \tag{2.18}$$

Having the ratio of those two velocities, the concentration can be calculated numerically. With the N-body simulations Millenium I and II the evolution of the concentration c of DM halos was studied. From the simple plot of the ratio of maximum and mean halo circular velocities as a function of mass, for which no particular density profile is required for the time being, it can be seen that the concentration of halos increases with the halo mass at higher redshifts, i.e. at high redshifts there is a flattening and upturn at the high-mass end. The data from the Millenium I and Millenium II simuation is illustrated in figure 2.3 [41].
The shape of the rotation curve depends strongly on the galaxy surface brightness. Galaxies with low-surface brightness do have slowly rising rotation curves, whereas for brighter ones the curve rises sharply and remains flat or in some cases declines beyond the optical radius R_{opt}. The disk mass-to-light-ratio has to increase with the luminosity with $(\frac{M}{L})_{disk} \propto L^{0.2}$ [42]. Halos of bright galaxies have masses, which are only weakly correlated to the luminosity. In addition, the halo circular velocity V_{200} is not proportional to the observed disk rotationspeed V_{opt}. Disks with a low rotationspeed ($V_{opt} < 150\frac{km}{s}$) have halos with higher circular velocity, while fast rotating disks ($V_{opt} > 150\frac{km}{s}$) are surrounded by halos with similar mass with $V_{200} = 200\frac{km}{s}$. This means that bright galaxies have halos with a lower circular velocity than the observed disk speed of rotation. The NFW profiles are also compatible with the observed rotation curves with the exception of low mass galaxies [42].

The exact distribution of the Dark Matter particles in Milky Way as well as in NGC 1068 is poorly known. The already described ΛCDM Model is very successful over a wide range of observation in today's cosmology and is considered as the Standard Model of Cosmology. In the mid 90s the resolution in N-body simulations got better and a discrepancy between observation and theoretical prediction arose. Simulations showed that the density of the DM halo increases rapidly towards the center with $\rho(r) \propto r^{\alpha}$, where α is between -1 and -1.5 [43]. However, such a cuspy

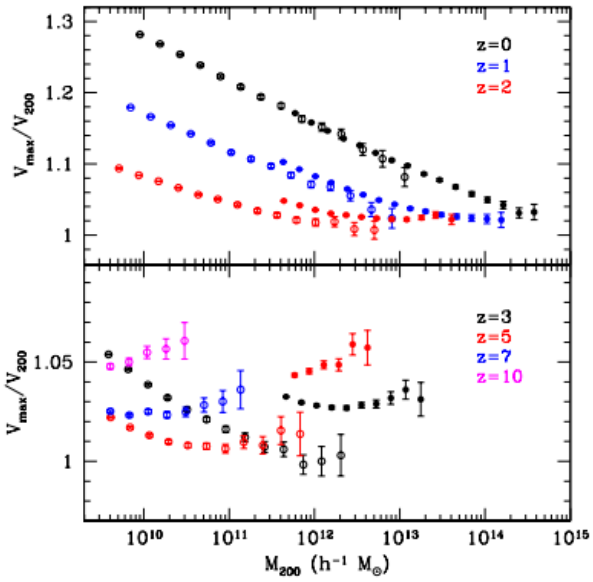

Figure 2.3: The ratio $\frac{V_{max}}{V_{200}}$ as a function of mass M_{200} for halos at different redshifts for MS-I (filled symbols) and MS-II (open sybols) simulations [41].

halo has not yet been observed. Galaxy rotation curves favor a constant density core in the Dark Matter distribution. This conflict is referred to as the "cusp-core-problem". A concrete example of this issue is shown in figure 2.4. Considering the rotation velocity of a spiral galaxy, the fit with a profile with a constant density core, in figure 2.4 the Isothermal, is better than a fit with cusp. The fundamental problem is that a profile with cusp, like the NFW profile, overestimates the rotation velocity by a factor of two in the inner few kiloparsecs [44].
However, the basic issues are not only the details on the density profiles, but the CDM theory assumes too much Dark Matter in this inner region. The largest deviation of predicted and observed rotation curves is obtained for small galaxies. In general, the majority of rotation curves are better fitted with a profile assuming a core, than NFW like profiles. This means a modifying of the profiles is necessary [44]. There are two possible solutions to this problem. One would be to change the nature of Dark Matter from cold, collisionless matter to self-interacting matter. Self-interacting DM leads to a core with constant density and isothermal dispersion. A second solution would be to keep the theory of Cold Dark Matter and refer to a gravitational interaction between Dark Matter and baryonic matter through stellar feedback [43].

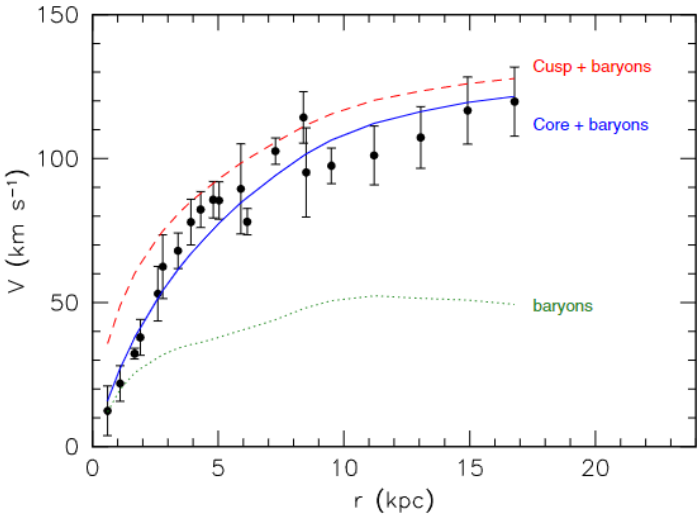

Figure 2.4: Cusp-Core-Problem. Measured rotation curve of F568-3 (points) compared with model fits assuming a core dark matter halo (blue solid curve) or a cuspy dark matter halo with a Navarro–Frenk–White profile (red dashedcurve, concentrationc=9:2,$V_{200} = 110\frac{km}{s}$) and dottet green line is distribution expected from the gravity of the stellar and gas components of the galaxy [44].

Even though there are discrepancies in observation and no proofed solution for the cusp-core problem exists, the standard density profile used in practice is the NFW profile. The NFW profile is also assumed in this thesis in order to compare the results with existing ones.

2.2.2 Detection of Dark Matter

Observational evidences have been made clear that DM exists. In order to deduce properties of DM, the detection is important. Even though no DM particle has been detected or observed yet, its nature similar to the ones enclosed by the SM has been agreed by physicist. There exist three different detection principles, which all consider an interaction between DM and SM: direct, indirect and collider searches. The according Feynman graphs are shown in figures 2.5, 2.6 and 2.7.

2.2.2.1 Direct Detection Method

The direct detection method is possible through the assumption of DM-SM scattering. The goal is to measure the DM-nucleon cross-section through the detection of

DM particles. The recoil of the nuclei, that it experiences after scattering, can be measured, which is used to differ background from an event signal. As the signal is expected to be low and rare, it is from great importance to reduce the background as good as possible. This is solved by putting such experiments deep in the underground [45] [46]. In order to even increase the sensitivity of the experiment to signals, materials with high atomic numbers are used. The Xenon experiment in the Gran Sasso Laboratory, for example, uses a liquid noble gas, Xenon, for the measurement of the recoil scintillation and ionization [47].

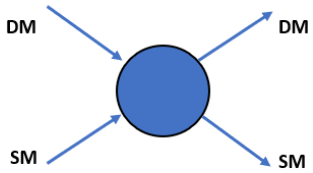

Figure 2.5: Direct detection through WIMP-SM scattering [45].

2.2.2.2 Indirect Detection Method

In contrast to direct detection, indirect detection aim to measure the energy spectrum of the SM particles, which are the products of annihilation or decay of Dark Matter particles. Signatures in gamma rays, neutrinos and antineutrinos and in antiparticles like positrons and antiprotons can be recognized. Successful detection of DM annihilation processes via indirect methods would specify its nature as a particle and give information of its properties, the annihilation cross-section or its mass, would be possible to determine [48]. The advantage of indirect detection is that no specific DM specialization needs to be done to the experiment, following an amount of observatories, which can strengthen or declare finding reports wrong very easily. In addition, Dark Matter models, which are not consistent with signatures in gamma-ray and cosmic-ray determined by the composition of SM particles from DM annihilation, can be rejected. Despite all those advantages the great challenge is to understand the astrophysical background well, in order to avoid problems. A problem could be the misinterpretation of a signal from the background of astrophysical source, since it can mimic a source of Dark Matter annihilation.
Experiments for indirect detection are ground based, as for example IceCube [2], or satellites particle detectors. Targets for such experiments are regions, where the density of DM is supposed to be high. Such targets are for example the galactic center or the galactic DM halo.

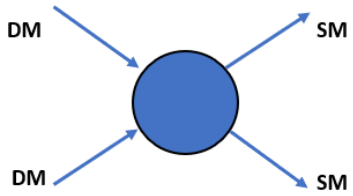

Figure 2.6: Indirect detection through WIMP self annihilation or decay [48].

2.2.2.3 Searches at Collider Experiments

In collider experiments it is assumed that SM particles can produce DM particles in collisions, by annihilation at high energies. Due to the weak interactions of WIMPs, they escape the detector and no visible signal is produced. The only way to search for them is via the measurement of the missing transverse energy and the resulting mass reconstruction. The momentum conservation states, that the net momentum must be the same before and after the collision. If there is an imbalance calculating the transverse momentum of all detected particles, this would be a signal for DM. Such experiments have already taken place and rise high expectation at several high energy colliders such as at the LHC at CERN or Tevatron at Fermilab [49].

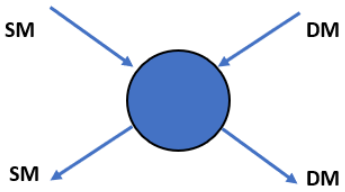

Figure 2.7: Collider detection through collision of SM particles [49]

However, despite tremendous experimental efforts, a signal for Dark Matter remains elusive and our understanding of the properties of Dark Matter is limited

2.2.2.4 Detection with IceCube

A detector for neutrinos, with the scientific objective of the indirect detection of Dark Matter, is located at the geographic South Pole near the Amundsen-Scott Station. The IceCube Neutrino Observatory is a cubic kilometer neutrino detector situated between 1450 m and 2450 m in the Arctic ice. It was completed in 2010 and

started up in 2011. The detection of astrophysical neutrinos and the identification of their sources, which was one of the main goals, was achieved in 2013 [50]. A schematic overview of the observatory is presented in figure 2.8.

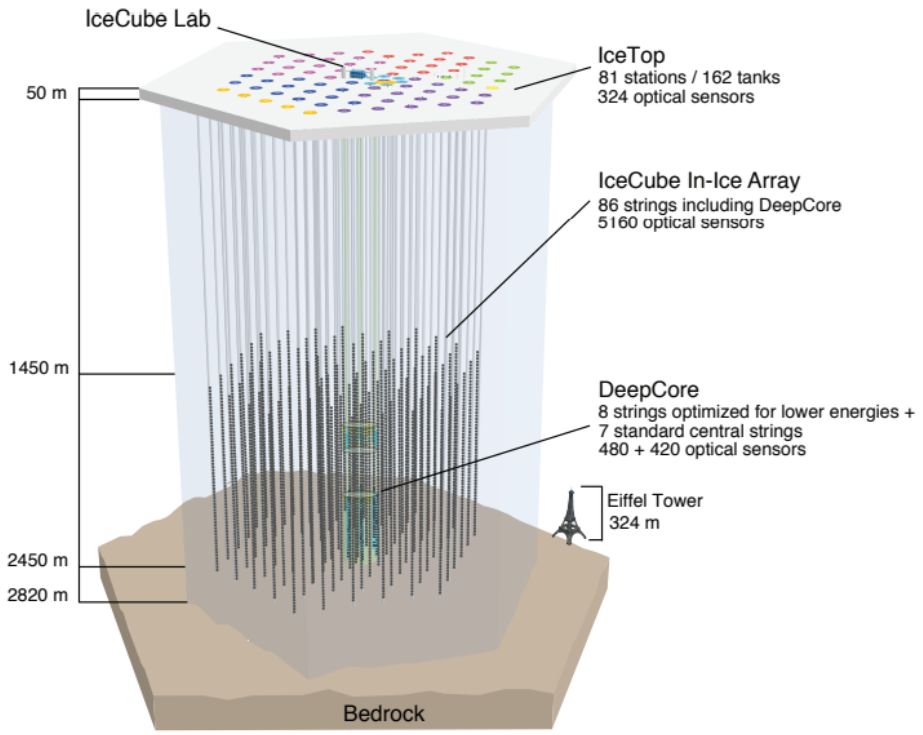

Figure 2.8: Schematic layout of the IceCube Neutrino Observatory with In-Ice array, DeepCore and IceTop [50].

IceCube can be subdivided in three parts: the IceTop, the In-Ice-Array and the DeepCore. In total there are 86 strings and 5160 digital optical modules (DOM), i.e. 60 DOMs on each string. The DOMs are the fundamental light sensor and data acquisition unit for IceCube. The In-Ice-Array consists of 78 strings, which are deployed within a hexagonal footprint on a triangular grid with 125 m horizontal spacing. The DOM-to-DOM distance is about 17 m. In the center 8 strings are deployed more compactly forming the DeepCore sub-detector, which are inserted deeper and have an average inter-string spacing of 72 m. 50 DOMs are placed between 2100 m and 2450m with a distance of 7m whereas the other 10 lie at deeps

shallower than 2000 m with a spacing of 10 m forming a veto cap. The DeepCore is optimized for low energies, i.e. for detecting neutrinos with energies between 10 GeV and 100 GeV. IceCube is therefore suited for the detection of neutrinos from WIMP Dark Matter annihilations in the GeV mass range. For cosmic air shower array, IceTop is located as the name already suggests on the surface and has the same grid as the In-Ice array, also with a central denser region. It consists of 162 ice tanks, respectively filled up to 0.9 m and arranged in 81 stations. Each of these tanks has two standard DOMs and one high and one low-gain DOM to allow higher dynamic range. The detection of neutrinos at IceCube is based on the Čherenkov effect [51]. Charged particles are created in neutrino interactions with molecules in the ice, which then move through the ice faster than light does. The charged leptons then emit Čherenkov radiation in form of photons, which are detected by the photomultipliers in the DOMs. The signal will then be digitized and transmitted to the laboratory. Because of the very small effective cross-section of neutrinos and the low fluxes expected at Earth, an enormously large detection volume is required. This condition is perfectly fulfilled by IceCube at the South Pole [50].

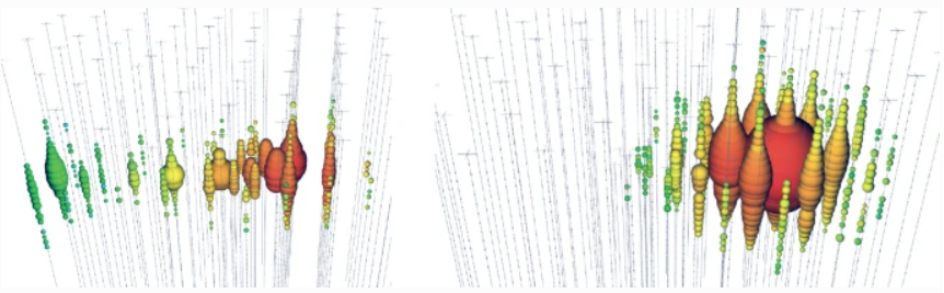

Figure 2.9: The two event topologies at IceCube: the track-like events (left) and cascade-like events (right) [52].

There are two different events, that represent the standard signatures of IceCube. Charged-current interactions of a high-energy muon neutrino and a nucleus, producing a hadron shower at the vertex, and an outgoing muon, are called track-like events. This is because the muon emits Čherenkov light along its track. This scenario is shown in figure 2.9 on the left. On the right side of the graphic, on the other hand, a so-called cascade event is shown. This is known as electromagnetic and hadronic shower from interactions of all neutrino flavours. The results for cascade like events are much more precise, because most of the showers are well-contained in the detector and also because the light output is directly proportional to the energy [52].

Chapter 3

Parametrization of the Dark Matter Halo of NGC 1068

The barred spiral galaxy NGC 1068, also called Messier 77, is an active galaxy with an active galactic nucleus (AGN). A picture of it taken by the Hubble Space Telescope can be seen in figure 3.1. It is in the constellation Cetus and is one of the best studied Seyfert galaxies. In February 2022, the supermassive black hole at its center, obscured by a ring of cosmic dust, was observed with the Very Large Telescope of ESO [53]. The galaxy has a mass of $M_{NGC1068} = 1 \cdot 10^9 M_\odot$, it is 14.4 Mpc away and is one of the biggest of Messier's catalogue with a major diameter of 7,1 arcmin and a minor of 6,0 arcmin. The physical major axis for the total magnitude 9.61 is $R_{tot} = 14.9$ kpc and for about 25.0 $\frac{\text{B-mag}}{\text{arcsec}^2}$ it is $R_{25} = 27.70$ kpc. The apparent magnitude amounts 8.9. The heliocentric radial velocity measures to $v = 1137 \frac{\text{km}}{\text{s}}$ and the redshift z is 0.003793 [54]. The geometry of NGC 1068 is illustrated in figure

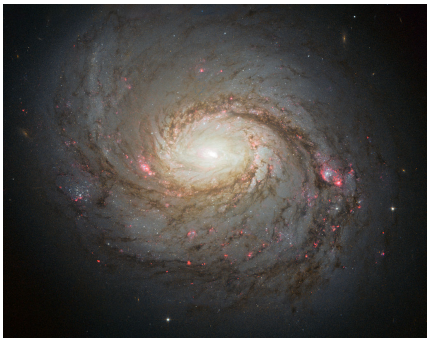

Figure 3.1: Picture of NGC 1068 core taken by Hubble Space Telescope [55].

3.2. The core radius is assumed to be 1 kpc. The spike radius is calculated to 2.43 pc for $\gamma = 1$ and 21.71 pc for $\gamma = 1.5$ [56][57].

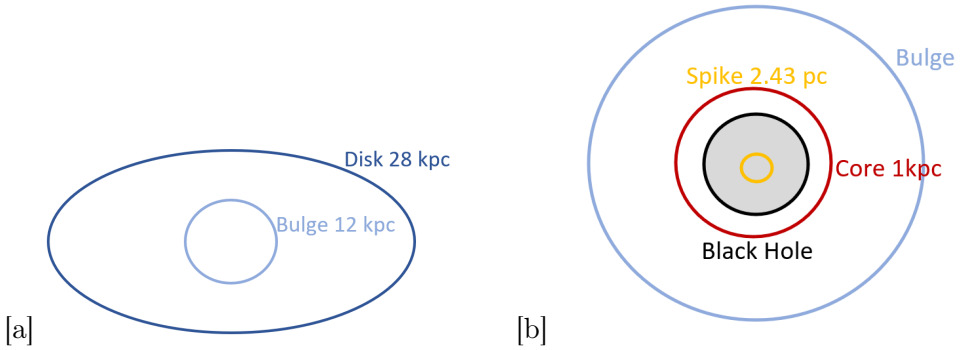

Figure 3.2: Assumed geometry of NGC 1068.

3.0.1 Parametrization of the Dark Matter Halo of NGC 1068 assuming a NFW density profile

Assuming a NFW halo density profile, the parameter R_s and ρ_s in equation 2.14 need to be determined for NGC 1068, in order to calculate the expected neutrino flux from the spike and disk of the galaxy. In general, two scenarios are noted as constraints for the halo density profile: a denser and smaller halo with a density slope $\gamma = 1.5$ for a radius $R_{200} = 14.91$kpc as an upper limit and a larger less denser one with the parameter $\gamma = 1$ and $R_{200} = 27.70$kpc as a lower limit. The evolution of the ratio of V_{max} and V_{200} is shown in figure 2.3, as a function of the mass M_{200} and the redshift z. With the assumption that the mass of NGC 1068 amounts $M_{NGC1068} = 1 \cdot 10^9 M_\odot$ and the redshift is approximately zero, the fraction can be determined by extrapolation of the data of the MS-II simulation for those conditions presented in chapter 2.2.1. This was done using the numpy polyfit function of degree 2 in Python. A value of $\frac{V_{max}}{V_{200}} = 1.3576$ was obtained. The halo concentration c can be determined numerically with equation 2.18 and with the result for the ratio $\frac{V_{max}}{V_{200}}$ to $c = 16.2737$.

The scale radius R_s can be calculated with equation 2.11 for the two mentioned scenarios. The value for $R_{200} = 14.91$kpc is $R_{s,\gamma=1.5} = 0.9162$kpc and for $R_{200} = 27.70$kpc is calculated to $R_{s,\gamma=1} = 1.7021$kpc. As the scale radius is determined and the mass of NGC 1068 is assumed as above, the density ρ_s can be calculated with formula 2.16, integrating over the NFW profile and rearranged to ρ_s. The results for the calculated parameters for both density slopes are shown in table 3.1.

Comparing these results with the numbers for the Milky Way, they are reason-

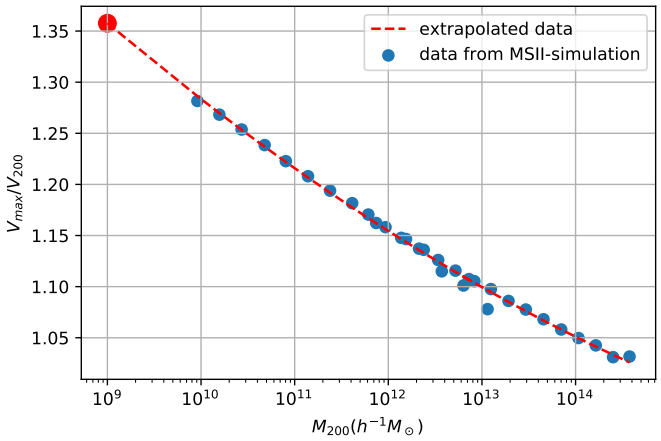

Figure 3.3: Extrapolated data (red) and value of $\frac{V_{max}}{V_{200}}$ for NGC 1068 (red point) for an assumed mass of $M_{NGC1068} = 1 \cdot 10^9 M_\odot$ and redshift approximated to zero from MSII-simulation data for z=0 (blue) [41].

Table 3.1: Calculated parameter for NGC 1068 with assumed NFW density profile for upper limit slope $\gamma = 1.5$ and lower limit slope $\gamma = 1$

density slope γ	scale radius R_s in [kpc]	density ρ_s in $[\frac{\text{kg}}{\text{m}^3}]$
1.5	0.9162	$1.0933 \cdot 10^{-21}$
1	1.7021	$5.8875 \cdot 10^{-22}$

able, as the difference is inside one magnitude, considering that NGC 1068 is a smaller galaxy. For the Milky Way ρ_s amounts about $0.24 \cdot 10^{-21} \frac{\text{kg}}{\text{m}^3}$ for $\gamma = 1$ [58].

3.0.2 Parametrization of the Dark Matter Halo of NGC 1068 assuming a NFW density profile including the Spike Profile

The further parametrization of the Dark Matter Halo includes the spike profile as well as the NFW profile, whereas the previous parameterization in chapter 3.1 only considers the NFW profile. The calculation for the NGC 1068 Halo is done as discussed in [56][57]. The profile including the Spike is shown for the density slope $\gamma = 1$ in figure 3.4. The density profile is:

$$\rho(R) = \begin{cases} 0, & r < R_{sch} \\ \frac{\rho_{sat} \cdot \rho_{sp}}{\rho_{sat} + \rho_{sp}}, & R_{sch} < r < R_{sp} \\ \rho_{NFW} & r > R_{sp} \end{cases} . \tag{3.1}$$

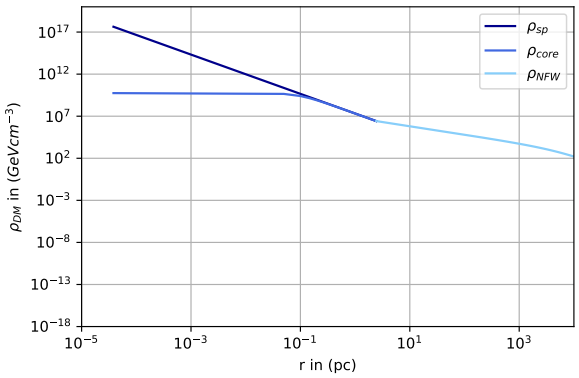

Figure 3.4: Density Profile of the Dark Matter Halo for NGC 1068 for the density slope $\gamma = 1$ assuming a NFW density profile including the Spike

The limit R_{Sch} is the Schwarzschildradius which is calculated with:

$$R_{Sch} = \frac{2G \cdot M_{BH}}{c^2} = 9.5571 \cdot 10^{-6}\text{pc} \tag{3.2}$$

where G is the gravitational constant and M_{BH} is the mass of the Black Hole, which amounts $10^8 M_\odot$. The Spike radius is chosen as discussed in [56]. For $\gamma = 1.5$ the Spike Radius amounts 21.71 pc and for $\gamma = 1$ it is 2.43 pc. ρ_{core} is calculated from the saturated density ρ_{sat} and the spike density ρ_{sp}. The density ρ_{sat} is determined by:

$$\rho_{sat} = \frac{m_\chi}{< \sigma v > \cdot t_{BH}} \tag{3.3}$$

with assumed lifetime of the Black Hole of 10^{10} years. The Spike density is:

$$\rho_{sp}(R) = \rho_s \cdot \left(\frac{R_{sp}}{R_s}\right)^{-\gamma} \cdot \left(\frac{R_{sp}}{R}\right)^{-\gamma_{sp}} \tag{3.4}$$

The values chosen for both density slopes are summarized in table 3.2.

Table 3.2: Calculated parameter for NGC 1068 with assumed NFW density profile for upper limit slope $\gamma = 1.5$ and lower limit slope $\gamma = 1$

density slope γ	scale radius R_s in [kpc]	density ρ_s in $[\frac{\text{GeV}}{\text{cm}^3}]$
1.5	10	4000
1	20	200

Chapter 4

Simulation of Neutrino Spectra from NGC 1068

Due to the lack of knowledge on Dark Matter annihilation production despite several experimental efforts, there is a great demand for numerical simulation programs. There are many theoretical models spanning a wide range of DM mass and interaction strength, making it difficult to study all possible scenarios. With comparisons of the maximum set of experimental results, it is possible to weed out the models that significantly deviate from current experiments. The simulations should help to simplify and optimize these by an efficient and model independent computation. In this thesis two different simulation softwares are used. The first one is the nummerical tool MadDM. The goal is to obtain observables, which are then set in in the second software called Pythia. In the following, general information, details on the programflow and the results are given for both of them.

4.1 Simulation with the Nummerical Tool MadDM

MadDM is a numerical tool, released in 2013, for the calculation of Dark Matter observables for generic new physics models. It includes the calculation for Dark Matter model predictions for relic density, direct and indirect detection [59].
The main goal was to provide the tools to compute Dark Matter observables. In addition, building a flexible platform together with MadGraph5 aMC@NLO (MG5 aMC) [60] to allow theorists, as well as experimentalists, to perform global fits of general Dark Matter models, in particular, using all the available technology to study physics beyond the Standard Model at colliders, was also of great interest. The first version of MadDM [61] provided a numerical tool for calculating relic density signals with collider observables for each model in UFO (Universal FeynRules Output [62] [63]) format. UFO is a format for automatized matrix-element generators, which goes beyond implicit assumptions like the color or Lorentz structure of a given model, the information on the model is encoded into a Python module. Direct detection was added in the second version [64]. From this point on, it was possible to compute nucleon cross-sections, Dark Matter double differential event rates of nuclear recoils

for a generic experiment, as well as the LUX (Large Underground Xenon [65]) experimental likelihood to compare with data. The third and latest version, which was also used for this work, additionally provides the tool for indirect detection calculations, thus achieving the goal for creating a platform for comprehensive Dark Matter studies. MadDM version 3.0 [59] is inheriting from MG5 aMC platform and so all features are integrated automatically. In addition, for user exists the possibility to change the parameters for the halo profile.
The indirect detection module probes the self-annihilation of DM in locally overdense regions. In order to compare the signal prediction to experimental data, the annihilation cross-section of Dark Matter and the energy spectrum of the messenger particles (neutrinos, gamma rays and cosmic rays) needs to be calculated. The module can be run in two different modes: fast and precise mode. The main difference is that the fast run mode is well suited for large samples in parameter space, where the precise mode computes each step of the indirect detection predictions with highest accuracy. An overview of the two running modes is given in figure 4.1.

		Indirect detection module		
		$< \sigma v >$	Energy Spectra	Flux at Earth
Running mode	Fast	$(\sigma \times v)\|_{v=v_{\mathrm{rel}}}$ Allows only DM DM → 2 particles	Numerical tables Allows only DM DM → SM SM	Prompt photons Neutrinos Positrons (fixed sets of propagation parameters)
	Precise	Full integration over the DM velocity distribution Allows for any DM annihilation process	Pythia 8 computes on the fly the energy spectra Allows for any DM annihilation process DM DM → n particles	Prompt photons Neutrinos Positrons Anti-protons (free choice of propagation parameters)

Figure 4.1: Overview of running modes 'fast' and 'precise' [59].

'Fast' mode only allows processes with two Dark Matter particles annihilating directly into two Standard Model particles (2→2). In general, no events are generated. The cross-section is calculated with a fast phase-space integrator using the Simpson method [66]. This means the leading order matrix elements annihilation processes are computed and integrated over the angle between the two final states. The cross-section then is evaluated at the required velocity. To obtain the energy spectra at the source, the cross-section is computed in fast mode and the PPPC4DMID numerical tabels [6], containing pre-computed results for annihilation into pairs of Standard Model particles only, are downloaded with (by default) or without elec-

troweak corrections. The spectra of different channels are combined according to their cross-sections.
In 'precise' mode, for the computation of the cross-section, two methods are available: reshuffeling and madevent. All the relevant subprocesses, given the annihilation processes, are identified by MG5 aMC, which then generates the amplitudes and the mappings needed for an efficient integration over the full phase-space. The phase-space integration is performed by MadEvent for both of the methods. Choosing the reshuffeling method implies: when the events have been generated, following the δ distribution for the velocity, a reshuffeling of the kinematic and of the weight of each event to map a Maxwell-Boltzmann velocity distribution is applied. In addition, a re-weightening of the matrix elements is put in with the consequence that every amplitude changes. In conclusion, this means that a Maxwell-Boltzmann distribution in velocity is taken into account computing the cross-section. In contrast, in the madevent option the cross-section is computed at a fixed Dark Matter velocity. This running mode works to compute automatically any possible leading order final annihilation state in a given DM model ($2\rightarrow$n if kinematically possible). The energy spectra at the source are then calculated with the generated events and PYTHIA 8 [67] for showering and hadronization. For the spectra at Earth the propagation is computed with the code DRAGON [59][68].

4.1.1 Simulation Details on MadDM

The goal of the simulation with MadDM is to obtain specific values, that can then be used in the subsequent simulation with Pythia. This is on the one hand the effective self-annihilation cross-section, and on the other hand the individual branching ratios of the assumed channels. The whole calculation is done for the three different dark matter masses: 100 GeV, 1 TeV and 10 TeV.
The first step is to select and import the Dark Matter model (database for all model at [69]). In this work the model DMsimp-s-spin0 was used. It describes a simplified DM model with s-channel mediater with spin equal to zero. It belongs to the collection of models, that are simple bottom-up extensions of the SM, obtained by adding a set of new particles and/or interactions to the Standard Model. The Dark Matter particle is assumed to be a Dirac particle by defining it as xd in the program. For the simulation it is important to calculate the relic density, as well as the indirect detection to get the desired values for Pythia. For this purpose, the relic density is generated and the indirect detection is added. These settings are all fixed in a generate text file.
In the launch text file then further parameters are set. The individual mass is defined, as well as the number of events, which depends on the choice of running mode. For 'fast' mode 10000 events are set, for 'precise' 10000000, in order to obtain a smooth spectrum. The simulation was performed for both modes and the

subsequent comparison of the results showed, that there was no difference between them and thus the 'fast' mode is already sufficiently accurate. Additionally, it is specified that the flux from indirect detection is only significant at the source in this work.

For the most accurate results, additional parameters in the parameter card are changed to the actual value, namely the masses of the charged leptons, the electron and the muon. Furthermore it is necessary to change the density profile in the maddm card to NFW and to modify the scale radius and density slope. The values for R_s and γ are used from the parameterization from the previous chapter 2.3.

4.1.2 Results of MadDM

The results files for the simulation with MadDM can be found in the appendix, see A.1, A.2, A.3. As already mentioned, the results for fast and precise running mode do not differ regarding the branching ratios and annihilation cross-sections. Following only results from fast mode are listed and inserted in the appendix.
Beginning with the annihilation cross-section into SM particle the relevant value, described as TotalSM-xsec in the file, is different for every considered mass as expected. For 100 GeV the number $6.89 \cdot 10^{-26} \frac{\mathrm{cm}^3}{\mathrm{s}}$ was obtained. About one magnitude higher is the value for an energy of 1 TeV with $5.71 \cdot 10^{-25} \frac{\mathrm{cm}^3}{\mathrm{s}}$. Last, as expected an even higher one for 10 TeV is obtained: $1.37 \cdot 10^{-23} \frac{\mathrm{cm}^3}{\mathrm{s}}$. The values listed are the upper limits for the total annihilation in SM particles cross-section given from MadDM, as the predicted are too low and probably obtained from unitary boundaries or cosmological limits, which do not make sense for this calculation.
The fraction of DM particles, which annihilate in an individual channel with respect to the total number of annihilating particles, the branching ratios, are given in percentage for several channels in the MadDM results. Included in MadDM are all annihilation channels of bosons (Z,W^{+-}, Higgs Boson H, γ) and the top quark. There is also an additional channel for DM annihilatiing in another form of DM. The ones important for this thesis and used in Pythia are listed in table 4.1.

Table 4.1: Results for branching ratios from MadDM simulation for 100 GeV, 1TeV and 10 TeV.

channel	100 GeV	1 TeV	10 TeV
52, -52 → 25, 25	0.00 %	0.13 %	1.86 %
52, -52→ 6, -6	0.00 %	73.84 %	10.85 %

4.2 Simulation of Neutrino Spectra using Pythia

Pythia is a computer program used in particle physics to simulate high energy collisions of elementary particles at accelerators, containing a coherent set of physics models for the evolution from a few-body hard-scattering process to a complex multiparticle final state. Pythia is the oldest and most widely used Monte Carlo event generator. The programming language is C++. A library of hard processes, models for initial- and final-state parton showers, matching and merging methods between hard processes and parton showers, multiparton interactions, beam remnants, string fragmentation and particle decays is part of the standard tool for the generation of events [67].
The goal of the simulation with Pyhia is to generate the neutrino energy spectra $\frac{dN_\nu}{dE}$ for each annihilation and Dark Matter mass taken into account. The program simulates the DM annihilation and resulting decay chain of the particle products. In this thesis the software package Pythia 8.2 is used [67].

4.2.1 Simulation Details on Pythia

A Dark Matter self-annihilation process can be considered as equivalent to the decay of a generic resonance, D, which has the double original DM mass $2m_\chi$. This is the result from the assumption of s-wave non-relativistic DM annihilation as discussed in Ref. [70]. The annihilation channels taken into account in this analysis are: $\chi\chi \to e^+e^-$, $\chi\chi \to \mu^+\mu^-$, $\chi\chi \to \nu\bar{\nu}$, $\chi\chi \to HH$ and $\chi\chi \to t\bar{t}$, considering a Dirac DM particle (PDG code 52). This is illustrated in figure 4.2. The branching ratios

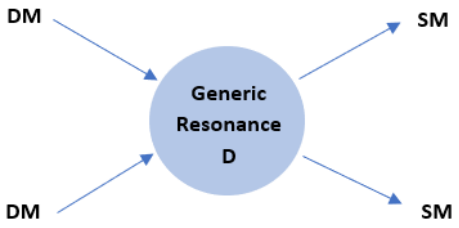

Figure 4.2: Shematic representation of the annihilation process considered in Pythia: Process equivalent to the decay into Standard Model particle (SM) of a generic resonance, D, which has the double dark matter mass $2m_\chi$, discussed in Ref. [70]

of the annihilation particle products, into which the resonance is forced to decay, are taken from the results of MadDM. Summing up all the branching ratios a total number of 100% results automatically. For unknown ratios 0.15 for the decay into e^+e^- and $\mu^+\mu^-$ and 0.1 for the decay into neutrinos was taken. In addition, the total

cross-section into Standard Model particles are taken from MadDM. The neutrinos produced in a simulated process are then recorded in a histogram according to their energies. Equivalently this is made for e^+e^-, $\mu^+\mu^-$ and photons. The energy spectra of $\mu^+\mu^-$, e^+e^-, photons and neutrinos for that particular annihilation process for the considered DM mass are obtained. The simulation is done for the masses 100 GeV, 1 TeV and 10 TeV. In order to obtain smooth energy spectra, especially a smooth neutrino spectra, a large number of events is necessary. In this thesis 10^6 annihilations are taken into consideration. For illustrating the energy spectra in a plot a Python code is applied.

Evaluating the first obtained data for the three spectra some problems arose. In Pythia the spectrum for a DM mass of 100 GeV was too imprecise to use and not what we expected. The mass of 100 GeV is approaching the mass of the mediator, which could lead to a decreasing accuracy. The simulation for the neutrino energy spectrum of 100 GeV was performed by another simulation software called χaroν [71] for muon neutrinos only. The results for 100 GeV were improved.
In order to get better values for the neutrino energy spectra of 1 and 10 TeV, e^+e^- as an annihilation channel and final state got cancelled in the Pythia simulation.

4.2.2 Results for Neutrino Energy Spectra using Pythia

From the simulation of the annihilation of DM into the postulated SM particles, the energy spectra of the assumed final states are obtained. In this case of $\mu^+\mu^-$, photons and neutrinos (see Appendix A.2 A.4, A.5 and A.6). For further calculations only the latter one is relevant, as the goal of this work is to calculate the neutrino flux from NGC 1068. The spectra for the respective DM masses can be seen in figures 4.3, 4.4, 4.5. It should be noted that the spectra are already normalized. As expected, there is a clear peak at the DM mass in each of the curves. Also the course of the curves of 1 TeV and 10 TeV are reasonable with the exception of the steep decrease of the counts short of the peak. For the 10 TeV spectrum it is more pronounced than for the 1 TeV spectrum. This issue was improved by using less final states as mentioned at the end of 4.2.1, but it could not be rejected completely. This may probably also come from the too low number of events.
To calculate the neutrino flux, the spectrum is integrated in order to obtain the number of neutrinos per annihilation. For the final results to match better to detector capability of the energy range, it is useful to start the integration for energies higher than 10 GeV (for the spectrum of DM mass of 100 GeV) and than 100 GeV (for 1 TeV and 10 TeV DM mass energy spectra). This is useful, because in the low energy ranges the simulation is very inaccurate and it is difficult to observe an event. Since the spectrum for a DM mass of 10 TeV already starts at 100 GeV, it is only necessary to cut the other two spectra. These are shown in figures 4.6 and 4.7. In the further

calculation the cut data is used for the DM masses m_χ= 100 GeV and m_χ=1 TeV. Due to the data from Pythia, the cut was made at 10.55 GeV and 110 GeV.

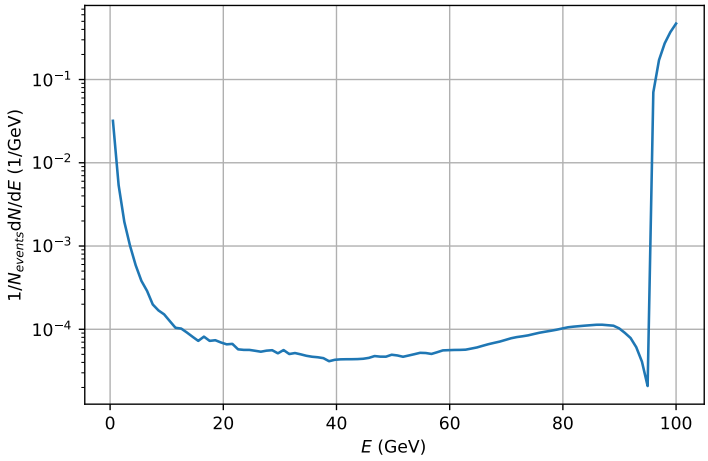

Figure 4.3: χaroν simulation on simple spin-0 DM annihilation, with a considered DM mass of 100 GeV. The self-annihilation cross-section and branch ratio setup is according to (4.2.1). In this simulation all secondary production (p^+_-, γ) from hadronic interaction is stored but only neutrinos production is shown here.

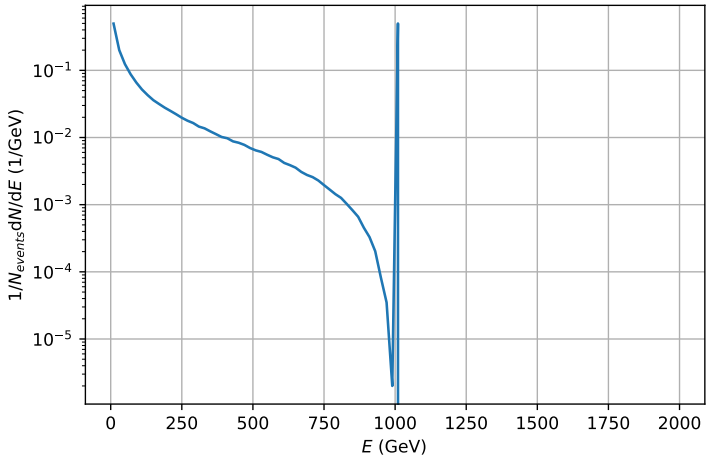

Figure 4.4: Pythia simulation on simple spin-0 DM annihilation, with a considered DM mass of 1 TeV. The self-annihilation cross-section and branch ratio setup is according to (4.2.1). In this simulation all secondary production (p^{+}_{-}, γ) from hadronic interaction is stored but only neutrinos production is shown here.

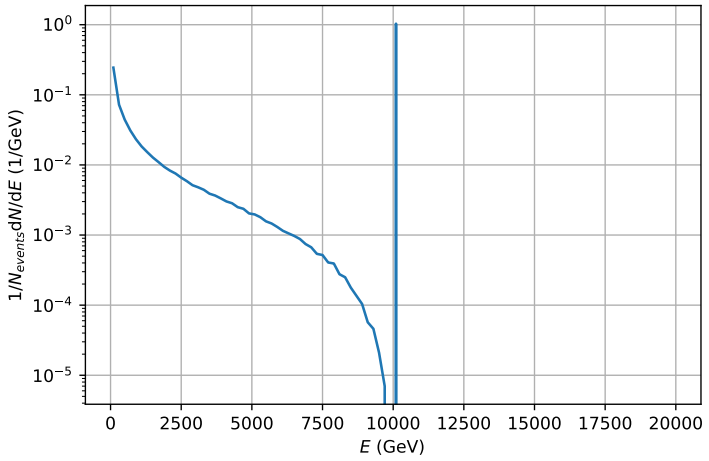

Figure 4.5: Pythia simulation on simple spin-0 DM annihilation, with a considered DM mass of 10 TeV. The self-annihilation cross-section and branch ratio setup is according to (4.2.1). In this simulation all secondary production (p^{+}_{-}, γ) from hadronic interaction is stored but only neutrinos production is shown here.

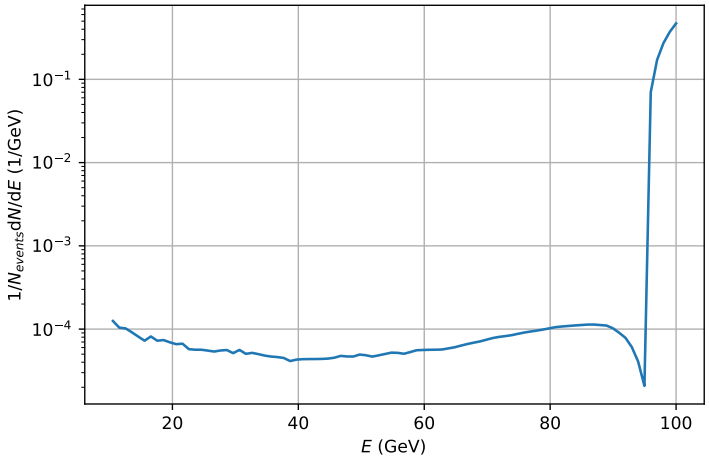

Figure 4.6: χaroν simulation on simple spin-0 DM annihilation, with a considered DM mass of 1 TeV. The self-annihilation cross-section and branch ratio setup is according to (4.2.1). In this simulation all secondary production (p^{+}_{-}, γ) from hadronic interaction is stored but only neutrinos production is shown here. For better match to detector capability of energy range, the data is cut at 10.55 GeV.

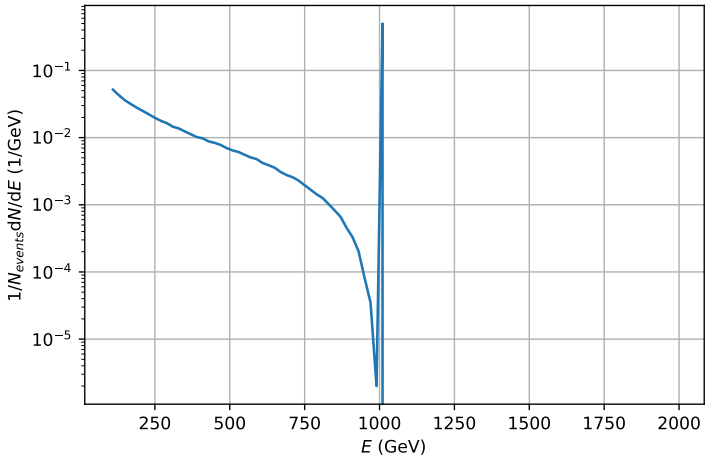

Figure 4.7: Pythia simulation on simple spin-0 DM annihilation, with a considered DM mass of 1 TeV. The self-annihilation cross-section and branch ratio setup is according to (4.2.1). In this simulation all secondary production (p^{+}_{-}, γ) from hadronic interaction is stored but only neutrinos production is shown here. For better match to detector capability of energy range, the data is cut at 110 GeV.

Chapter 5

Calculation of Neutrino Flux from Dark Matter Annihilation from NGC 1068

5.1 Galactic Contribution

The expected neutrino flux from NGC 1068 is determined analogously to the calculation performed for the Milky Way with the specific parameters for NGC 1068 [7][8].
Due to the black hole at the center of the Milky Way and NGC 1068, the Dark Matter is redistributed into a spike. How luminous the spike is depends on the density distribution in the halo. Whereas halos with finite core have inconspicuous spikes, cuspy halos have such bright spikes, that one gets important limits for the density slope from the detected neutrino signals. The annihilation rate is significantly increased in the spike, since it is associated with the squared matter density ρ_m^2 and highest near the inner radius of it, because of the steep spike profile. The course of the density in the spike depends not only on the distribution in the halo, i.e. the slope of the inner halo γ, but also on the behavior of the initial phase space density. Considered are models with inner cusps, where the phase space density diverges, from which follows a spike slope greater than or equal to three halves ($\gamma_{Sp} \geq \frac{3}{2}$). If the WIMP is considered as a self-annihilating DM particle, it is assumed to enter the spike due to gravitational interactions. The total neutrino flux is the sum of the flux of the halo and the spike [7].

$$\Phi_\nu^{total} = \Phi_\nu^{halo} + \Phi_\nu^{spike} \tag{5.1}$$

For the spike one obtains with an assumed power law profile:

$$\Phi_\nu^{spike} = \frac{\rho_s^2 Y_\nu \langle \sigma v \rangle R_s}{m_\chi^2} \left(\frac{R_{Sp}}{R_s} \right)^{3-2\gamma} \left(\frac{R_{Sp}}{R_{in}} \right)^{2\gamma_{Sp}-3} \tag{5.2}$$

The parameter ρ_s and R_s are the specific from the choice of the density profile, determined in chapter 3. The number of neutrinos produced per annihilation is set in Y_ν and $\langle \sigma v \rangle$ is the thermal averaged annihilation cross-section. m_χ corresponds to

the DM mass, in this case to the mass of the WIMP. The density slope γ is defined as in chapter 2.2.1 and γ_{sp} refers to the density slope in the spike and can be calculated by

$$\gamma_{sp} = (9 - 2 \cdot \gamma)/(4 - \gamma) \tag{5.3}$$

ρ_{core} is the maximal density, which is set by annihilation in the inner region of the spike and depends on the age of the black whole, namely t_{bh}. This core has a radius $R_{core} = R_{Sp}(\rho_R/\rho_{core})^{1/\gamma_{Sp}}$ with ρ_R calculated from the power law profile 3.3. R_{Sp} is the Spike radius and R_{in} is defined by:

$$R_{in} = 1.5[(20R_S)^2 + R_{core}^2]^{0.5} \tag{5.4}$$

Including the spike the flux increases by five orders of magnitude for cusped halos [7].

The second component is the flux expected from the disk. The differential $\frac{d\Phi_\nu^{halo}}{dE_\nu}$ depends on the WIMPs's thermal averaged annihilation cross-section, $\langle\sigma v\rangle$, on the inverse of the WIMP mass squared, m_χ. It is also proportional to the yield of neutrinos of each annihilation process, $\frac{dN_\nu}{de}$, and the line-of-sight integral for DM, the J-factor, namely [8]:

$$\frac{d\Phi_\nu^{halo}}{dE_\nu} = \frac{1}{4\pi}\frac{\sigma v}{\kappa m_\chi^2}\frac{1}{3}\frac{dN_\nu}{dE_\nu}J(\Omega) \tag{5.5}$$

The variable κ corresponds to the properties of the DM particle. If DM is assumed to be a Dirac particle κ is equal 4. If DM is a Majorana particle, which means that the particle and its antiparticle do not differ from each other, κ is set equal 2. In this thesis a Dirac DM particle is considered, like in the simulations. The energy spectrum $\frac{dN_\nu}{dE_\nu}$ for the annihilation into two neutrinos is simply:

$$\frac{dN_\nu}{dE_\nu} = 2\delta(1 - \frac{E}{m_\chi})\frac{m_\chi}{E^2} \tag{5.6}$$

However, the spectrum has no analytic form, they were simulated with Pythia and can be replaced here. The final component $J(\Omega)$ is referred to as the J-factor, which is a three-dimensional integral over the distance dx along the line of sight of the squared density profile and solid angle $d\Omega$.

$$J(\Omega) = \int d\Omega \int\limits_{l.o.s.} \rho_\chi^2(x)dx \tag{5.7}$$

The total flux is the integration over the energy E in equation 5.5.

Another annihilation signal comes from the isotropic backgroundflux of extragalactic

halos. Integrating the DM annihilation over all redshifts we get a diffuse isotropic neutrino signal, which comes on the one hand from the background flux of the diffuse DM distribution, whose rate increases with $\Omega_{DM}^2 \sim (1+z)^6$ and on the other hand from the latetime distribution of the large overdensities of the halos. In general, this is neglectable [8].

5.2 Results for the Neutrino Flux from NGC 1068 assuming a NFW density profile

With the results from Pythia at this point it is possible to calculate the neutrino flux from the spike and disk of NGC 1068. As not the differential, but the total flux is from great interest, the fist step in the calculation needs to be the integration of the the spectra dN/dE.
The integration is done by summing up over the energy bins times the corresponding energy. In detail, the difference ΔE is multiplied with each value for dN/dE and the sum of all those bins was taken to obtain the total number of neutrinos. In order to get the number per annihilation a normalization is necessary, which has already done by in 4.2.2 by dividing $\frac{dN}{dE}$ by the number of events chosen. In addition a propagation of 99% is assumed.

5.2.1 Neutrino Flux from the Spike assuming a NFW density profile

The neutrino flux from the spike from DM annihilation can be determined according to equation 5.2 for the upper limit $\gamma = 1.5$ and lower limit $\gamma = 1$ of the density slope. All parameters used for the calculation are summarized in table 5.2. The density ρ_s and the scale radius R_s are chosen correspondingly to γ, according to the calculation in chapter 3.1. The annihilation cross-section is taken from MadDM for the considered masses m_χ equal to 100 GeV, 1 TeV and 10 TeV. The total number of neutrinos per annihilation Y_ν is calculated from the spectra of Pythia. With equation 5.3 the density slope of the spike can be determined. The value for the spike radius R_{sp} are 21.71 pc ($\gamma = 1.5$) and 2.43 pc ($\gamma = 1$). The core radius R_{core} is set o 1 kpc, see figure 3.2, following, R_{in} results from equation 5.4. The final values for each density slope and all masses are summarized in table 5.1.

5.2.2 Neutrino Flux from Disk assuming a NFW density profile

The results for the neutrino flux from the disk can now be calculated according to equation 5.5. A summary of all parameters used, is given in table 5.4. In general, equation 5.5 is written in a differential form. However, since the total flux is of interest, the spectrum is integrated analogously to the calculation of the neutrino flux of the spike, i.e. the number of neutrinos per annihilation is determined. The

Table 5.1: Results for the neutrino flux from the spike calculated with eq. 5.2 in and parameters in 5.2 for DM masses 100 GeV, 1 TeV and 10 TeV for both scenarios $\gamma = 1.5$ and $\gamma = 1$.

	100 GeV	1 TeV	10 TeV
flux in $[1/cm^2$ s GeV] for $\gamma = 1.5$	$2.5740 \cdot 10^{-14}$	$2.9754 \cdot 10^{-14}$	$1.1975 \cdot 10^{-13}$
flux in $[1/cm^2$ s GeV] for $\gamma = 1$	$4.7614 \cdot 10^{-19}$	$5.5038 \cdot 10^{-19}$	$6.2083 \cdot 10^{-18}$

Table 5.2: Parameters used in the calculation for neutrino flux from Spike, equation 5.2.

	$\gamma = 1.5$	$\gamma = 1$
ρ_s	$0.6132 \frac{\text{GeV}}{\text{cm}^3}$	$0.3302 \frac{\text{GeV}}{\text{cm}^3}$
R_s	0.9162 kpc	1.7021 kpc
m_χ	100 GeV	100 GeV
	1 TeV	1 TeV
	10 TeV	10 TeV
σv	$6.89 \cdot 10^{-26} \frac{\text{cm}^3}{s}$	$6.89 \cdot 10^{-26} \frac{\text{cm}^3}{s}$
	$5.71 \cdot 10^{-25} \frac{\text{cm}^3}{s}$	$5.71 \cdot 10^{-25} \frac{\text{cm}^3}{s}$
	$1.37 \cdot 10^{-23} \frac{\text{cm}^3}{s}$	$1.37 \cdot 10^{-23} \frac{\text{cm}^3}{s}$
Y_ν	1.3534	1.3534
	18.8774	18.8774
	316.6665	316.6665
R_{sp}	21.71 pc	2.43 pc
γ_{sp}	2.4	2.3

annihilation cross-sections $\langle \sigma v \rangle$, as well as the masses m_χ, are chosen as in the calculation before (5.2.1).The parameter κ is set equal to 4, as a Dirac DM particle is considered. An important role in the calculation of the flux from the disk plays the J-factor. It is determined according to equation 5.7 for both cases: $\gamma = 1.5$ and $\gamma = 1$. The integration over the whole sphere and along the virial radius is assumed, namely:

$$J(\Omega) = 4\pi \cdot \int_1^{R_{200}} \rho^2_{NFW}(r) dr$$

As the NFW halo density profile has an infinite core, the integral is divergent for the lower integration limit equal zero. It starts here at 1 kpc to avoid this problem. The final numbers for the neutrino flux per annihilation from the disk of NGC 1068 are entered in table 5.3.

Table 5.3: Results for the neutrino flux from the disk calculated with eq. 5.5 in and parameters in 5.4 for DM masses 100 GeV, 1 TeV and 10 TeV for both scenarios $\gamma = 1.5$ and $\gamma = 1$.

	100 GeV	1 TeV	10 TeV
flux in $[1/cm^2$ s GeV] for $\gamma = 1.5$	$1.6159 \cdot 10^{-10}$	$1.8679 \cdot 10^{-10}$	$7.5177 \cdot 10^{-10}$
flux in $[1/cm^2$ s GeV] for $\gamma = 1$	$5.4803 \cdot 10^{-11}$	$6.3349 \cdot 10^{-11}$	$2.4597 \cdot 10^{-10}$

Table 5.4: Parameters used in the calculation for neutrino flux from Disk, equation 5.5.

	$\gamma = 1.5$	$\gamma = 1$
m_χ	100 GeV	100 GeV
	1 TeV	1 TeV
	10 TeV	10 TeV
σv	$6.89 \cdot 10^{-26} \frac{\text{cm}^3}{s}$	$6.89 \cdot 10^{-26} \frac{\text{cm}^3}{s}$
	$5.71 \cdot 10^{-25} \frac{\text{cm}^3}{s}$	$5.71 \cdot 10^{-25} \frac{\text{cm}^3}{s}$
	$1.37 \cdot 10^{-23} \frac{\text{cm}^3}{s}$	$1.37 \cdot 10^{-23} \frac{\text{cm}^3}{s}$
Y_ν	1.3534	1.3534
	18.8774	18.8774
	316.6665	316.6665
κ	4	4
$J(\Omega)$	$2.6131 \cdot 10^{21} \frac{\text{GeV}^2}{\text{cm}^5}$	$8.8624 \cdot 10^{20} \frac{\text{GeV}^2}{\text{cm}^5}$

5.3 Results for the Neutrino Flux from NGC 1068 assuming a NFW density profile including the Spike profile

5.3.1 Neutrino Flux from the Spike assuming a NFW density profile including the Spike Profile

In this section the results for the neutrino Flux from the Spike including a Spike profile are presented. The main difference to the above listed numbers are the change of parameters regarding the characteristic density ρ_s and the scale radius R_s, which are chosen correspondingly to chapter 3.2. The remaining numbers are equally used as in chapter 5.1.1. All the numbers for the calculation are summarized in table 5.6. The final results for the neutrino flux from the Spike are in 5.7.

Table 5.5: Results for the neutrino flux from the spike calculated with eq. 5.2 in and parameters in 5.6 for DM masses 100 GeV, 1 TeV and 10 TeV for both scenarios $\gamma = 1.5$ and $\gamma = 1$ including the Spike profile in the parametrization of the Dark Matter Halo of NGC 1068.

	100 GeV	1 TeV	10 TeV
flux in $[1/cm^2$ s GeV] for $\gamma = 1.5$	$1.6230 \cdot 10^{-7}$	$1.8761 \cdot 10^{-7}$	$7.5509 \cdot 10^{-7}$
flux in $[1/cm^2$ s GeV] for $\gamma = 1$	$2.8783 \cdot 10^{-15}$	$3.3271 \cdot 10^{-15}$	$3.8442 \cdot 10^{-14}$

Table 5.6: Parameters used in the calculation for neutrino flux from Spike, equation 5.2 including the Spike profile in the parametrization of the Dark Matter Halo of NGC 1068.

	$\gamma = 1.5$	$\gamma = 1$
ρ_s	$4000 \frac{\text{GeV}}{\text{cm}^3}$	$200 \frac{\text{GeV}}{\text{cm}^3}$
R_s	10 kpc	20 kpc
m_χ	100 GeV	100 GeV
	1 TeV	1 TeV
	10 TeV	10 TeV
σv	$6.89 \cdot 10^{-26} \frac{\text{cm}^3}{s}$	$6.89 \cdot 10^{-26} \frac{\text{cm}^3}{s}$
	$5.71 \cdot 10^{-25} \frac{\text{cm}^3}{s}$	$5.71 \cdot 10^{-25} \frac{\text{cm}^3}{s}$
	$1.37 \cdot 10^{-23} \frac{\text{cm}^3}{s}$	$1.37 \cdot 10^{-23} \frac{\text{cm}^3}{s}$
Y_ν	1.3534	1.3534
	18.8774	18.8774
	316.6665	316.6665
R_{sp}	21.71 pc	2.43 pc
γ_{sp}	2.4	2.3

5.3.2 Neutrino Flux from the Disk assuming a NFW density profile including the Spike profile

The calculation for the flux from the disk is done according to eq. 5.5. The parameters are used according to chapter 3.2 and summarized in table 5.8. The results mainly vary from the results in chapter 5.1.2 due to the different J-factor. The Spike profile is included here. The density in the inner region, including the Schwartzschild radius is 0. The density profile of the Spike extents to the Spike radius. Beyond the Spike Radius the dark matter density profile is the existing NFW profile. $J(\Omega)$ is

calculated with:

$$J(\Omega) = 4\pi \cdot \left(\int_0^{R_{Sch}} 0dr + \int_{R_{Sch}}^{R_{sp}} \rho^2_{core}(r)dr + \int_{R_{sp}}^{R_{gal}} \rho^2_{NFW}(r)dr \right) \tag{5.8}$$

The Spike radius is chosen according to chapter 3 for the two density slopes. ρ_{core} is calculated from the saturated density ρ_{sat} and the spike density ρ_{sp}.

$$\rho_{core} = \frac{\rho_{sat} \cdot \rho_{sp}}{\rho_{sat} + \rho_{sp}} \tag{5.9}$$

The density ρ_{sat} is determined by eq. 3.3 with an assumed lifetime of the Black Hole of 10^{10} years. The Spike density is calculated with equation 3.4. The upper limit R_{gal} of the NFW-integral amounts 200 kpc, which includes the whole mass of the Galaxy NGC 1068. The final results for the neutrino flux from the disk are presented in table 5.5.

Table 5.7: Results for the neutrino flux from the disk calculated with eq. 5.5 in and parameters in 5.8 for DM masses 100 GeV, 1 TeV and 10 TeV for both scenarios $\gamma = 1.5$ and $\gamma = 1$.

	100 GeV	1 TeV	10 TeV
flux in $[1/cm^2$ s GeV] for $\gamma = 1.5$	$1.2041 \cdot 10^8$	$1.8728 \cdot 10^8$	$1.8960 \cdot 10^8$
flux in $[1/cm^2$ s GeV] for $\gamma = 1$	$3.2466 \cdot 10^6$	$5.0415 \cdot 10^6$	$5.1292 \cdot 10^6$

Table 5.8: Parameters used in the calculation for neutrino flux from Disk, equation 5.5.

	$\gamma = 1.5$	$\gamma = 1$
m_χ	100 GeV	100 GeV
	1 TeV	1 TeV
	10 TeV	10 TeV
σv	$6.89 \cdot 10^{-26} \frac{\text{cm}^3}{s}$	$6.89 \cdot 10^{-26} \frac{\text{cm}^3}{s}$
	$5.71 \cdot 10^{-25} \frac{\text{cm}^3}{s}$	$5.71 \cdot 10^{-25} \frac{\text{cm}^3}{s}$
	$1.37 \cdot 10^{-23} \frac{\text{cm}^3}{s}$	$1.37 \cdot 10^{-23} \frac{\text{cm}^3}{s}$
Y_ν	1.3534	1.3534
	18.8774	18.8774
	316.6665	316.6665
κ	4	4
$J(\Omega)$	$1.9472 \cdot 10^{39} \frac{\text{GeV}^2}{\text{cm}^5}$	$5.2502 \cdot 10^{37} \frac{\text{GeV}^2}{\text{cm}^5}$
	$2.6200 \cdot 10^{39} \frac{\text{GeV}^2}{\text{cm}^5}$	$7.0530 \cdot 10^{37} \frac{\text{GeV}^2}{\text{cm}^5}$
	$6.5905 \cdot 10^{38} \frac{\text{GeV}^2}{\text{cm}^5}$	$1.7829 \cdot 10^{37} \frac{\text{GeV}^2}{\text{cm}^5}$

Chapter 6

Conclusion

From our calculation it is notable, that even with a high slope, the flux from the spike is several magnitudes lower than the flux from the disk. As a conclusion, this means that the super massive Black Hole itself may not be the main source of high neutrinos flux from NGC 1068. Regarding absorption, the matter overdense has an inevitable influence on the gamma-ray propagation, which could be able to explain the absence of a gamma-ray signal from NGC 1068.
For the final conclusion the results from the calculation including the Spike profile are used as they are better. In order to compare the data from the simulation with the data from IceCube, the flux at source is translated to the flux at earth by including the distance of NGC 1068 to earth and calculating the effective area of the detector (https://github.com/mhuber89/Plenum). The events number detected are calculated by integrating over the flux and the effective area.

$$n_{det} = \int\int \frac{d\Phi}{dE} \cdot A_{eff} d\Omega dE \tag{6.1}$$

As a result from the simulation with a dark matter mass of 10 TeV , the events number detected $n_{det} = 2.877 \cdot 10^{-27^{+5}_{-5}}$ is obtained for a ten years analysis by IceCube. The error of two magnitudes is assumed because of the blazar and AGN properties of NGC 1068. In this calculation the diffuse flux is determined, whereas NGC 1068 is a Galaxy with an Active Galactic Nucleus (AGN) with the jet pointing to earth (Blazar). In addition it follows a uncertainty from the calculation of the effective area of one magnitude. Another error, which is included, is the uncertainty of the J-factor, $\pm 10^2$ is assumed. Comparing the results from the simulation with Pythia and the calculation of the neutrino flux, with the experimentally obtained numbers from the IceCube experiment, some conclusions can be drawn. In general, the parameter of the mean number of astrophysical neutrino events associated with a given point in the sky $\hat{\mu}_{ns}$, in this case NGC1068, and the spectral index $\hat{\gamma}$ fully define the (anti-) neutrino flux $\Phi_{\nu+\bar{\nu}}$, which can be expressed by the power-law: $\Phi_{\nu+\bar{\nu}} = \Phi_0 \left(\frac{E_\nu}{E_0}\right)^{-\gamma}$. The free parameter Φ_0 is the flux normalization for the neutrino energy of E_0=1 TeV.
The ten years of IceCube point-like neutrino sources paper suggests a potential to

detect the signal from NGC 1068 with $\hat{n}_s$=50.4 and the spectrum index $\hat{\gamma} = 3.2$ [3]. In order to give a possible physical explanation to the experimental data, we compare our simulation results with the IceCube given spectrum shape.
Plotting the resulting power-law distribution for the differential flux with the parameters from IceCube and comparing them with the simulation results for the galactic distribution [8] for a Dark Matter mass of 10 TeV, a similar slope is notable. This is presented in figure 6.1.

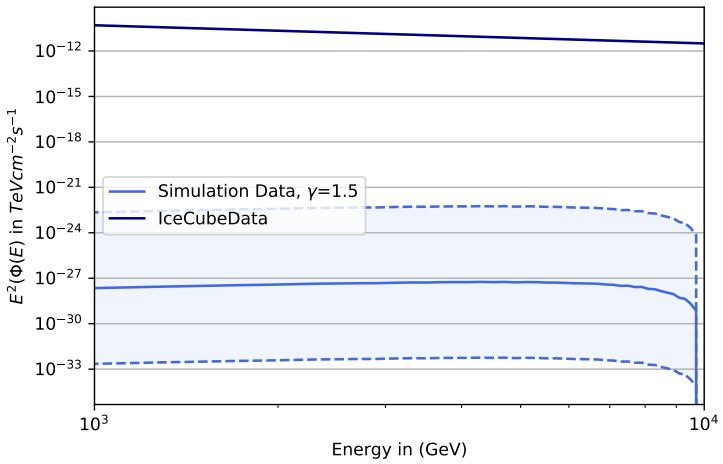

Figure 6.1: Comparison of differential flux of power-law distribution with IceCube parameter ($\hat{\gamma} = 3.2$ and $\Phi_0 = 5.0 \cdot 10^{-11}\text{TeV}^{-1}\text{cm}^{-2}\text{s}^{-1}$ and of galactic distribution with simulation results for the flux at earth (γ=1) for a dark matter mass of 10 TeV.

We can say, the TeV Dark Matter Annihilation scenario has no conflict on spectrum shape from NGC 1068. Therefore, DM can be one of the potential explanation of the neutrino flux from NGC 1068.

Appendix A

Simulation Details

A.1 MadDM Results

A.1.1 100 GeV

```
################################################
#                MadDM v. 3.2                  #
################################################


################################################
# Relic Density                                #
################################################

Omegah2                       = 2.66e+03
Omegah_Planck                 = 1.20e-01
xsi                           = 1.00e+00        # xsi = (Omega/Omega_Planck)
x_f                           = 1.00e+01
sigmav_xf                     = 7.41e-31        # cm^3 s^-1
# % of the relic density channels
%_52.-52>25.25                = 0.00 %
%_52.-52>22.22                = 74.05 %
%_52.-52>54.54                = 0.00 %
%_52.-52>23.23                = 0.13 %
%_52.-52>6.-6                 = 0.00 %
%_52.-52>24.-24               = 3.20 %
%_52.-52>22.23                = 22.62 %

################################################
# Indirect Detection                           #
################################################
# Results in brackets display [prediction, upper limit]

# Annihilation cross section computed with the method: inclusive
# <sigma v>[cm^3 s^-1] of continuum spectrum final states and Fermi dSph limits (if available, else -1)
52.-52>6.-6                   = [0.00e+00,1.00e-15]
52.-52>24.-24                 = [2.42e-40,2.80e-26]
52.-52>54.54                  = [0.00e+00,-1.00e+00]
52.-52>23.23                  = [8.94e-42,2.82e-26]
52.-52>25.25                  = [0.00e+00,1.00e-15]

# Global Fermi dSph Limit computed with PPPC4DMID_ew spectra
TotalSM_xsec                  = [2.51e-40,6.89e-26]
Fermi_Likelihood              = -1.76e+01
Fermi_pvalue                  = 1.16e-07

################################################
# CR Flux at Earth [particles cm^-2 s^-1 sr^-1) #
################################################

# Fluxes calculated using the spectra from PPPC4DMID_ep

Flux_neutrinos_e              = 2.22e-26
Flux_neutrinos_mu             = 2.43e-26
Flux_neutrinos_tau            = 2.19e-26
Flux_gammas                   = 6.78e-26
```

Figure A.1: MadDM results file for simulation for 100 GeV.

A.1.2 1 TeV

```
################################################
#                MadDM v. 3.2                  #
################################################


################################################
# Relic Density                                #
################################################

Omegah2                       = 2.56e-01
Omegah_Planck                 = 1.20e-01
xsi                           = 1.00e+00        # xsi = (Omega/Omega_Planck)
x_f                           = 2.20e+01
sigmav_xf                     = 9.53e-27        # cm^3 s^-1
# % of the relic density channels
%_52.-52>25.25                = 0.13 %
%_52.-52>22.22                = 2.48 %
%_52.-52>54.54                = 21.43 %
%_52.-52>23.23                = 0.36 %
%_52.-52>6.-6                 = 73.84 %
%_52.-52>24.-24               = 0.26 %
%_52.-52>22.23                = 1.51 %

################################################
# Indirect Detection                           #
################################################
# Results in brackets display [prediction, upper limit]

# Annihilation cross section computed with the method: inclusive
# <sigma v>[cm^3 s^-1] of continuum spectrum final states and Fermi dSph limits (if available, else -1)
52.-52>6.-6                   = [1.73e-34,2.02e-25]
52.-52>24.-24                 = [6.12e-37,2.32e-25]
52.-52>54.54                  = [3.85e-38,-1.00e+00]
52.-52>23.23                  = [8.31e-37,2.27e-25]
52.-52>25.25                  = [3.02e-37,1.85e-25]

# Global Fermi dSph Limit computed with PPPC4DMID_ew spectra
TotalSM_xsec                  = [1.75e-34,5.71e-25]
Fermi_Likelihood              = -1.76e+01
Fermi_pvalue                  = 3.20e-05

################################################
# CR Flux at Earth [particles cm^-2 s^-1 sr^-1) #
################################################

# Fluxes calculated using the spectra from PPPC4DMID_ep

Flux_neutrinos_e              = 2.39e-22
Flux_neutrinos_mu             = 2.37e-22
Flux_neutrinos_tau            = 2.16e-22
Flux_gammas                   = 2.60e-21
```

Figure A.2: MadDM results file for simulation for 1 TeV.

A.1.3 10 TeV

```
################################################
#                 MadDM v. 3.2                 #
################################################


################################################
# Relic Density                                #
################################################

Omegah2                       = 8.13e+00
Omegah_Planck                 = 1.20e-01
xsi                           = 1.00e+00         # xsi = (Omega/Omega_Planck)
x_f                           = 2.10e+01
sigmav_xf                     = 2.43e-28         # cm^3 s^-1
# % of the relic density channels
%_52.-52>25.25                = 1.86 %
%_52.-52>22.22                = 34.92 %
%_52.-52>54.54                = 22.25 %
%_52.-52>23.23                = 5.11 %
%_52.-52>6.-6                 = 10.85 %
%_52.-52>24.-24               = 3.72 %
%_52.-52>22.23                = 21.30 %

################################################
# Indirect Detection                           #
################################################
# Results in brackets display [prediction, upper limit]

# Annihilation cross section computed with the method: inclusive
# <sigma v>[cm^3 s^-1] of continuum spectrum final states and Fermi dSph limits (if available, else -1)
52.-52>6.-6                   = [1.02e-36,3.52e-24]
52.-52>24.-24                 = [3.49e-37,8.38e-24]
52.-52>54.54                  = [2.10e-36,-1.00e+00]
52.-52>23.23                  = [4.80e-37,7.45e-24]
52.-52>25.25                  = [1.75e-37,4.67e-24]

# Global Fermi dSph Limit computed with PPPC4DMID_ew spectra
TotalSM_xsec                  = [2.03e-36,1.37e-23]
Fermi_Likelihood              = -1.76e+01
Fermi_pvalue                  = 6.49e-07

################################################
# CR Flux at Earth [particles cm^-2 s^-1 sr^-1) #
################################################

# Fluxes calculated using the spectra from PPPC4DMID_ep

Flux_neutrinos_e              = 2.75e-24
Flux_neutrinos_mu             = 9.80e-25
Flux_neutrinos_tau            = 1.08e-24
Flux_gammas                   = 7.50e-25
```

Figure A.3: MadDM results file for simulation for 10 TeV.

A.2 Pythia Results

A.2.1 100 GeV

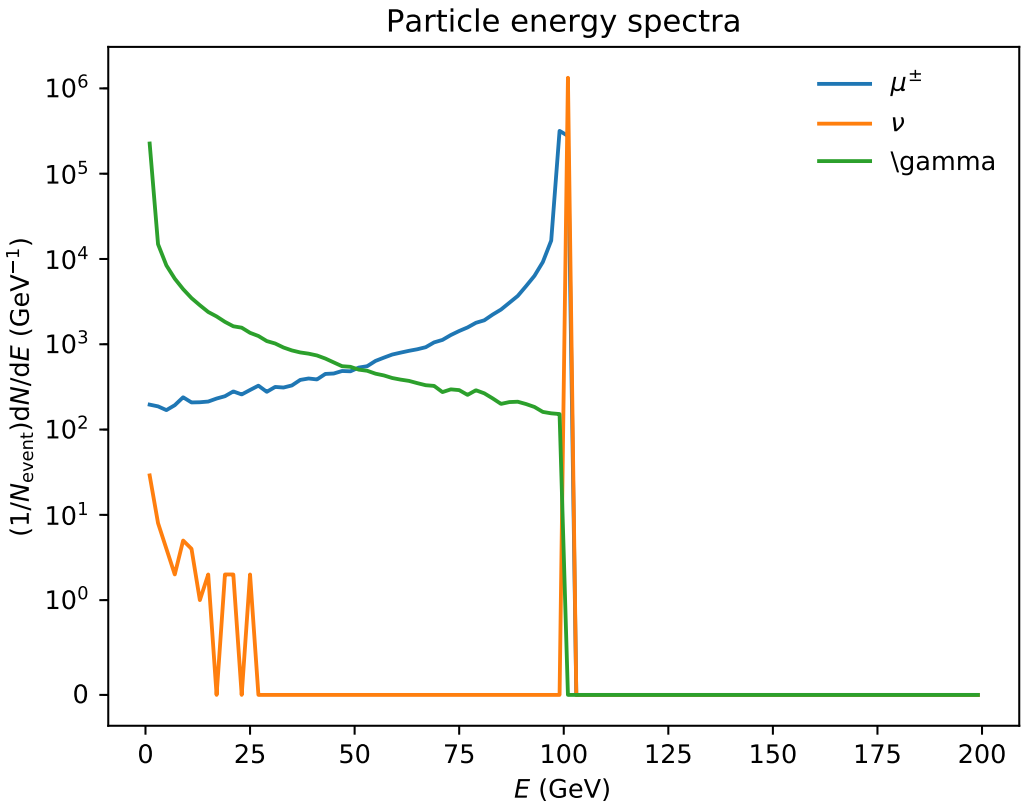

Figure A.4: Pythia results for energy spectrum of $\mu^+\mu^-$, neutrinos ν and photons γ for simulation for 100 GeV.

A.2.2 1 TeV

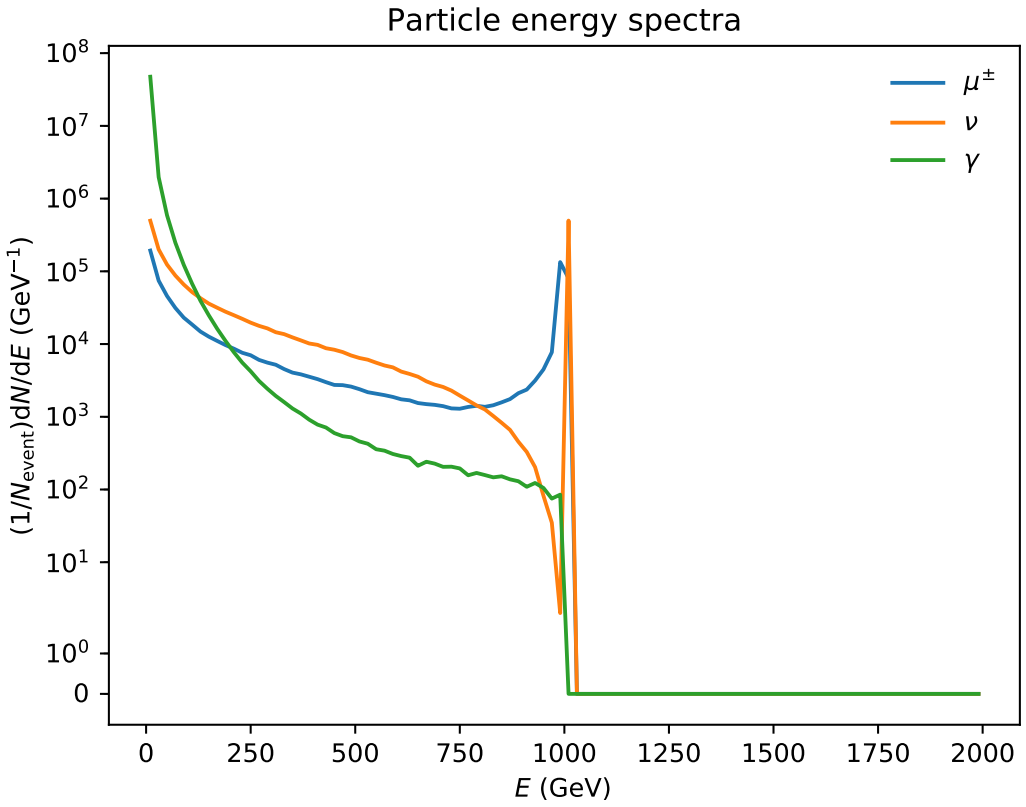

Figure A.5: Pythia results for energy spectrum of $\mu^+\mu^-$, neutrinos ν and photons γ for simulation for 1 TeV.

A.2.3 10 TeV

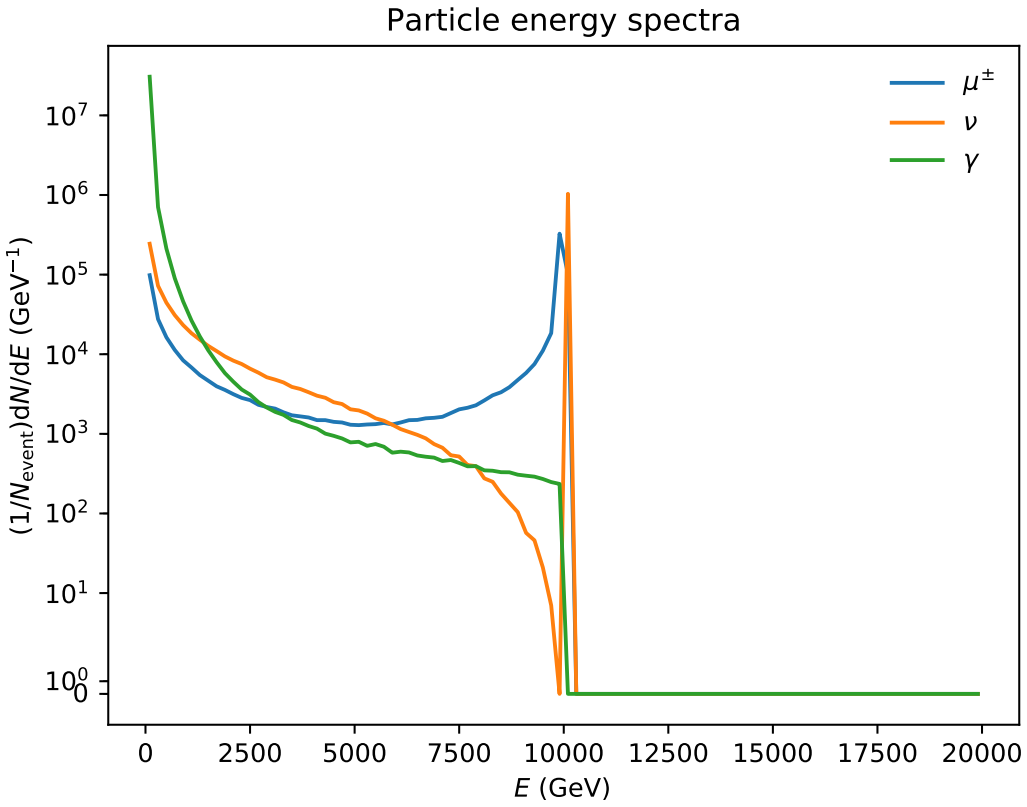

Figure A.6: Pythia results for energy spectrum of $\mu^+\mu^-$, neutrinos ν and photons γ for simulation for 10 TeV.

Bibliography

[1] National Aeronautics and Space Administration- NASA Official: Dr. Edward J. Wollack. *What is the Universe made of.* Accessed:2022-09-01. URL: %5Curl%7Bhttps://wmap.gsfc.nasa.gov/universe/uni_matter.html%7D.

[2] Dr. Martin Wolf. *Indirect Searches for Dark Matter in the Milky Way with IceCube-DeepCore.* Department of Physics, Stockholm University, Sweden, 2016. ISBN: 978-91-7649-401-1.

[3] M. G. Aartsen et al. »Time-Integrated Neutrino Source Searches with 10 Years of IceCube Data«. In: *Physical Review Letters* 124.5 (2020). DOI: 10.1103/physrevlett.124.051103. URL: https://doi.org/10.1103%2Fphysrevlett.124.051103.

[4] S. Abdollahi et al. »iFermi/i Large Area Telescope Fourth Source Catalog«. In: *The Astrophysical Journal Supplement Series* 247.1 (2020), p. 33. DOI: 10.3847/1538-4365/ab6bcb. URL: https://doi.org/10.3847$%5C%2F1538-4365%5C%$2Fab6bcb.

[5] Elisa Resconi, Ralph Engel and Thomas K. Gaisser. *Cosmic Ray and Particle Physics second Edition.* 2016th ed. Cambridge University Press. Chap. 11. ISBN: 978-1-139-19219-4.

[6] Marco Cirelli et al. »PPPC 4 DM ID: a poor particle physicist cookbook for dark matter indirect detection«. In: *Journal of Cosmology and Astroparticle Physics* 2011.03 (2011), pp. 051–051. DOI: 10.1088/1475-7516/2011/03/051. URL: https://doi.org/10.1088$%5C%2F1475-7516%5C%2F2011%5C%2F03%5C%$2F051.

[7] Paolo Gondolo and Joseph Silk. »Dark matter annihilation at the galactic center«. In: (1999). arXiv: 9906391 [astro-ph].

[8] Carlos A. Arguelles et al. »Dark matter annihilation to Neutrinos«. In: (2021). arXiv: 1912.09486 [hep-ph].

[9] Franz Zwicky. »Die Rotverschiebung von extragalaktischen Nebeln«. In: (1933).

[10] Friedrich Bessel. »On the variations of the proper motions of Procyon and Sirius«. In: *Monthly Notices of the Royal Astronomical Society, Vol. 6, p.136-141* (1844). eprint: https://doi.org/10.1093/mnras/6.11.136.

[11] Gianfranco Bertone and Dan Hopper. »A History of Dark Matter«. In: (2016). arXiv: 1605.04909v2 [astro-ph].

[12] V. C. Rubin, W. K. J. Ford and N. Thonnard. »Rotational properties of 21 SC galaxies with a large range of luminosities and radii, from NGC 4605 (R=4kpc) to UGC 2885 (R=122kpc)«. In: (1980). eprint: https://doi.org/10.1086/158003.

[13] Edvige Corbelli and Paolo Salucci. »The Extended Rotation Curve and the Dark Matter Halo of M33«. In: (1999). arXiv: 9909252 [astro-ph].

[14] A. Bosma. »The distribution and kinematics of neutral hydrogen in spiral galaxies of various morphological types«. In: (1978). eprint: http://ned.ipac.caltech.edu/level5/March05/Bosma/frames.html.

[15] Boris V. Alexeev. »To the Theory of Galaxies Rotation and the Hubble Expansion in the Frame of Non-Local Physics «. In: *Journal of Modern Physics, 2012, 3, 1103-1122* (2012). eprint: https://doi.org/10.4236/jmp.2012.329145.

[16] Douglas Clowe et al. »A direct empirical proof of the existence of dark matter«. In: (2006). arXiv: 0608407 [astro-ph].

[17] Maruša Bradač et al. »Strong and Weak Lensing United. III. Measuring the Mass Distribution of the Merging Galaxy Cluster 1ES 0657-558«. In: *The Astrophysical Journal* 652.2 (2006), pp. 937–947. DOI: 10.1086/508601. URL: https://doi.org/10.1086%2F508601.

[18] The MACHO Collaboration. »The MACHO Project: Limits on Planetary Mass Dark Matter in the Galactic Halo from Gravitational Microlensing«. In: (1996). arXiv: 9604176 [astro-ph].

[19] M. Milgrom. »A modification of the Newtonian dynamics as a possible alternative to the hidden mass hypothesis.« In: *Astrophysical Journal, Vol. 270, p. 365-370* (1983).

[20] M. Jiang et al. »Search for axion-like dark matter with spin-based amplifiers«. In: (2021). arXiv: 2102.01448 [hep-ph].

[21] Dan Hopper and Stefano Profumo. »Dark Matter and Collider Phenomenology of Universal Extra Dimensions«. In: (2007). arXiv: 0701197v2 [hep-ph].

[22] H. E. Haber et al. »The search for supersymmetry: Probing physics beyond the standard model«. In: (1985).

[23] G. Jungmana, M. Kamionkowski and K. Griest. »Supersymmetric Dark Matter«. In: (1995). arXiv: 9506380v1 [hep-ph].

[24] Y. Fukuda et al. »Evidence for Oscillation of Atmospheric Neutrinos«. In: *Physical Review Letters* 81.8 (1998), pp. 1562–1567. DOI: 10.1103/physrevlett.81.1562. URL: https://doi.org/10.1103$%5C%$2Fphysrevlett.81.1562.

[25] Q. R. Ahmad et al. »Direct Evidence for Neutrino Flavor Transformation from Neutral-Current Interactions in the Sudbury Neutrino Observatory«. In: *Physical Review Letters* 89.1 (2002). DOI: 10.1103/physrevlett.89.011301. URL: https://doi.org/10.1103%2Fphysrevlett.89.011301.

[26] Bodgan Povh et al. *Teilchen und Kerne*. 9., VERB. AUFL., 2014. Springer-Verlag, pp. 139–181. ISBN: 978-3-642-37821-8.

[27] Jaan Einasto. »On Galactic Descriptive Functions«. In: (1996).

[28] Andrea Albert et al. »Search for 100 MeV to 10 GeV -raylines in the Fermi-LAT data and implications for gravitino dark matter in the $\mu\nu$SSM«. In: (2014). arXiv: 1406.3430 [astro-ph.HE].

[29] James E. Gunn and J. Richard Gott. »On Galactic Descriptive Functions«. In: (1972).

[30] E. Battaner and E. Florido. »The rotation curve of spiral galaxies and its cosmological implications«. In: (2000). arXiv: 0010475 [astro-ph].

[31] Andreas Burkert. »The Structure of Dark Matter Haloes in Dwarf Galaxies«. In: (1995). arXiv: 9504041 [astro-ph].

[32] Cosmos-Swinburne University of Technology. *Virial Theorem*. Accessed:2022-09-01. URL: %5Curl%7Bhttps://astronomy.swin.edu.au/cosmos/v/Virial+Theorem#:~:text=The$%5C%20virial%5C%20theorem%5C%20relates%5C%20the,energy%5C%2C%5C%20U%5C%20of%5C%20the%5C%20body$%7D.

[33] Zu-Gan Deng Wen-Hao Liu Yan-Ning Fu and Jie-Hao Huang. »An Equilibrium Dark Matter Halo with the Burkert Profile«. In: (2005). arXiv: 0505579 [astro-ph].

[34] Jaan Einasto. »On the Construction of a Composite Model for the Galaxy and on the Determination of the System of Galactic Parameters«. In: (1995).

[35] J.F. Navarro et al. »The inner structure of CDM haloes- III. Universality and asymptotic slopes«. In: (2004). arXiv: 0311231 [astro-ph].

[36] Eric Hayashi and Simon D.M. White. »Understanding the halo-mass and galaxy-mass cross-correlation functions«. In: (2008).

[37] Barun Kumar Dhar and Liliya L.R. williams. »Surface brightness and intrinsic luminosity of ellipticals«. In: (2012).

[38] E. Retana-Montenegro et al. »Analytical properties of Einasto dark matter halos«. In: (2012). arXiv: 1202.5242 [astro-ph].

[39] Julio F. Navarro, Carlos S. Frenk and Simon D.M. White. »The Structure of Cold Dark Matter Halos«. In: (1996). arXiv: 9508025 [astro-ph].

[40] Julio F. Navarro, Carlos S. Frenk and Simon D.M. White. »A Universal Density Profile from Hierarchical Clustering«. In: (1997). arXiv: 9611107 [astro-ph].

[41] F. Prada et al. »Halo concentrations in the standard ΛCDM cosmology«. In: (2011). arXiv: 1104.5130 [astro-ph].

[42] Julio F. Navarro. »The Cosmological Significance of Disk Galaxy Rotation Curves«. In: (1998). arXiv: 9807084 [astro-ph].

[43] Yong Shi et al. »A cuspy dark matter halo«. In: (2021). arXiv: 2101.01282 [astro-ph].

[44] D. H. Weinberg et al. »Cold dark matter: controversies on small scales«. In: (2013). arXiv: 1306.0913 [astrp-ph].

[45] Teresa Marrodan Undagoitia and Ludwig Rauch. »Dark matter direct-detection experiments«. In: (2017). arXiv: 1509.08767.

[46] Marc Schumann. »Direct Detection of WIMP Dark Matter:Concepts and Status«. In: (2019). arXiv: 1903.03026.

[47] J. Angle et al. »First Results from the XENON10 Dark Matter Experiment at the Gran Sasso National Laboratory«. In: *Phys. Rev. Lett.* 100 (2 2008), p. 021303. DOI: 10.1103/PhysRevLett.100.021303. URL: https://link.aps.org/doi/10.1103/PhysRevLett.100.021303.

[48] Carlos Pérez de los Heros. »Status of direct and indirect dark matter searches«. In: (2020). arXiv: 2001.06193.

[49] Stefano Giagu. »WIMP Dark matter searches with the ATLAS detector at the LHC«. In: (2019).

[50] The IceCube Collaboration. »The IceCube Neutrino Observatory: Instrumentation and Online Systems«. In: (2017). arXiv: 1612.05093 [astro-ph].

[51] Bodgan Povh et al. *Teilchen und Kerne*. 9., VERB. AUFL., 2014. Springer-Verlag, p. 415. ISBN: 978-3-642-37821-8.

[52] Markus Ahlers, Klaus Helbing and Carlos Pérez de los Heros. »Probing Particle Physics with IceCube«. In: (2018). arXiv: 1806.05696 [astro-ph.HE].

[53] MAX-PLANCK$_G$*ESELLSCHAFT*. *Schwarzes Loch im Staubring-Forschende beobachten das Zentrum der aktiven Galaxie NGC 1068*. Accessed:2022-09-01. URL: %5Curl%7Bhttps://www.mpg.de/18274805/schwarzes-loch-in-ngc1068%7D.

[54] Caltech University. *NASA/IPAC EXTRAGALACTIC DATABASE*. Accessed:2022-09-01. URL: %5Curl%7Bhttps://ned.ipac.caltech.edu/cgi-bin/objsearch?search_type=Obj_id&objid=58240&objname=1&img_stamp=YES&hconst=73.0&omegam=0.27&omegav=0.73&corr_z=1%7D.

[55] NASA/ESA. *Hubble observes the hidden depths of Messier 77*. Accessed:2022-09-01. URL: %5Curl%7Bhttps://esahubble.org/news/heic1305/%7D.

[56] Francesc Ferrer, Gonzalo Herrera and Alejandro Ibarra. *New constraints on the dark matter-neutrino and dark matter-photon scattering cross sections from TXS 0506+056*. 2022. DOI: 10.48550/ARXIV.2209.06339. URL: https://arxiv.org/abs/2209.06339.

[57] Thomas Lacroix et al. »Unique probe of dark matter in the core of M87 with the Event Horizon Telescope«. In: *Physical Review D* 96.6 (2017). DOI: 10.1103/physrevd.96.063008. URL: https://doi.org/10.1103%2Fphysrevd.96.063008.

[58] Fabrizio Nesti and Paolo Salucci. »The Dark Matter Halo of the Milky Way, AD 2013«. In: (2013). arXiv: 1304.5127 [astro-ph].

[59] Frederice Ambrogia et al. »MadDM v.3.0: a Comprehensive Tool for Dark Matter Studies«. In: (2019). arXiv: 1804.00044v2 [hep-ph].

[60] J. Alwall et al. »The automated computation of tree-level and next-to-leading order differential cross sections, and their matching to parton shower simulations«. In: *Journal of High Energy Physics* 2014.7 (July 2014). DOI: 10.1007/jhep07(2014)079. URL: https://doi.org/10.1007$%5C%2Fjhep07%5C%282014%5C%29079$.

[61] Mihailo Backović, Kyoungchul Kong and Mathew McCaskey. »MadDM v.1.0: Computation of dark matter relic abundance using MadGraph 5«. In: *Physics of the Dark Universe* 5-6 (2014), pp. 18–28. DOI: 10.1016/j.dark.2014.04.001. URL: https://doi.org/10.1016$%5C%$2Fj.dark.2014.04.001.

[62] Adam Alloul et al. »FeynRules 2.0 — A complete toolbox for tree-level phenomenology«. In: *Computer Physics Communications* 185.8 (2014), pp. 2250–2300. DOI: 10.1016/j.cpc.2014.04.012. URL: https://doi.org/10.1016%2Fj.cpc.2014.04.012.

[63] Céline Degrande et al. »UFO – The Universal FeynRules Output«. In: *Computer Physics Communications* 183.6 (2012), pp. 1201–1214. DOI: 10.1016/j.cpc.2012.01.022. URL: https://doi.org/10.1016$%5C%$2Fj.cpc.2012.01.022.

[64] Mihailo Backović et al. »Direct detection of dark matter with MadDM v.2.0«. In: *Physics of the Dark Universe* 9-10 (2015), pp. 37–50. DOI: 10.1016/j.dark.2015.09.001. URL: https://doi.org/10.1016%2Fj.dark.2015.09.001.

[65] D.S. Akerib et al. »The Large Underground Xenon (LUX) experiment«. In: *Nuclear Instruments and Methods in Physics Research Section A: Accelerators, Spectrometers, Detectors and Associated Equipment* 704 (2013), pp. 111–126. DOI: 10.1016/j.nima.2012.11.135. URL: https://doi.org/10.1016%2Fj.nima.2012.11.135.

[66] Stefan Weinzierl. *Introduction to Monte Carlo methods*. 2000. DOI: 10.48550/ARXIV.HEP-PH/0006269. URL: https://arxiv.org/abs/hep-ph/0006269.

[67] Torbjorn Sjostranda et al. »An Introduction to PYTHIA 8.2«. In: (2014). arXiv: 1410.3012 [hep-ph].

[68] Chiara Arina et al. »Studying dark matter with MadDM 3.1: a short user guide«. In: (2020). arXiv: 2012.09016v1 [hep-ph].

[69] *FeynRules model database*. Accessed:2022-09-01. URL: %5Curl%7Bhttp://feynrules.irmp.ucl.ac.be/wiki/ModelDatabaseMainPage%7D.

[70] Marco Cirelli et al. »Model-independent implications of the e+, e-, anti-proton cosmic ray spectra on properties of Dark Matter«. In: (2008). arXiv: 0809.2409v1 [hep-ph].

[71] Qinrui Liu et al. »χaroν: a tool for neutrino flux generation from WIMPs«. In: (2020). arXiv: 2007.15010 [hep-ph].